



澳門大學  
UNIVERSIDADE DE MACAU  
UNIVERSITY OF MACAU

# Outstanding Academic Papers by Students

## 學生優秀作品



# **Adaptive Fourier Decomposition Approach to ECG Denoising**

by

**Ze Wang**

Final Year Project Report submitted in partial fulfillment  
of the requirements for the Degree of

**Bachelor of Science in Electrical and Electronics Engineering**

**2014**



**Faculty of Science and Technology  
University of Macau**

\*\*\*\*\* Bachelor's Thesis Quote \*\*\*\*\*

**Bachelor's Thesis (or Final Report of Design Project II)**

In presenting this Final Report of Project (ELEC402) in partial fulfillment of the requirements for a Bachelor's Degree at the University of Macau, I agree that the **UM Library and Faculty of Science and Technology (FST)** shall make its copies available strictly for internal circulation or inspection. No part of this thesis can be reproduced by any means (electronic, mechanical, visual, and etc.) before the valid date (usually less than 3 years) limit listed below. Copying of this thesis before the valid date from other parties is allowable **only** under the prior written permission of the author(s).

Printed name: Wang, Ze Signature: \_\_\_\_\_

Student number: DB029068 Date: 2014/5/19

Reliable Contact information (address, tel. no., email, etc.) of author:

Tel. No.: 62917848

Email: wangze19910407@gmail.com

Valid date until 2017/5/18

\*\*\*\*\* End of Bachelor's Thesis Quote \*\*\*\*\*

## ABSTRACT

In this work, a novel signal decomposition method named Adaptive Fourier Decomposition (AFD) is investigated, which can decompose signals to some mono-components that only contain positive phase derivatives based on their energy distributions. With such nice characteristics, the AFD is applied removing noise from ECG signals. More specifically, a judgment is defined based on the estimated signal-to-noise ratio of a noisy signal to stop the recursive AFD process, with which a novel AFD-based denoising algorithm is proposed for ECG signals. In validation, artificial and real ECG signals from the MIT-BIH Arrhythmia Database with additive Gaussian white noise, muscle and electrode motion artifacts are used. Moreover, four other denoising methods based on the Fourier transform, the wavelet transform, the empirical mode decomposition and the ensemble empirical mode decomposition are used to compare with the AFD-based denoising method. The simulation results indicate that the proposed AFD-based method performs mostly the best. In addition, from the simulation study, two rules of the AFD are concluded which can be used to choose and adjust the decomposition level of the AFD for denoising. In summary, this report shows that the AFD is a promising tool for ECG signal denoising.

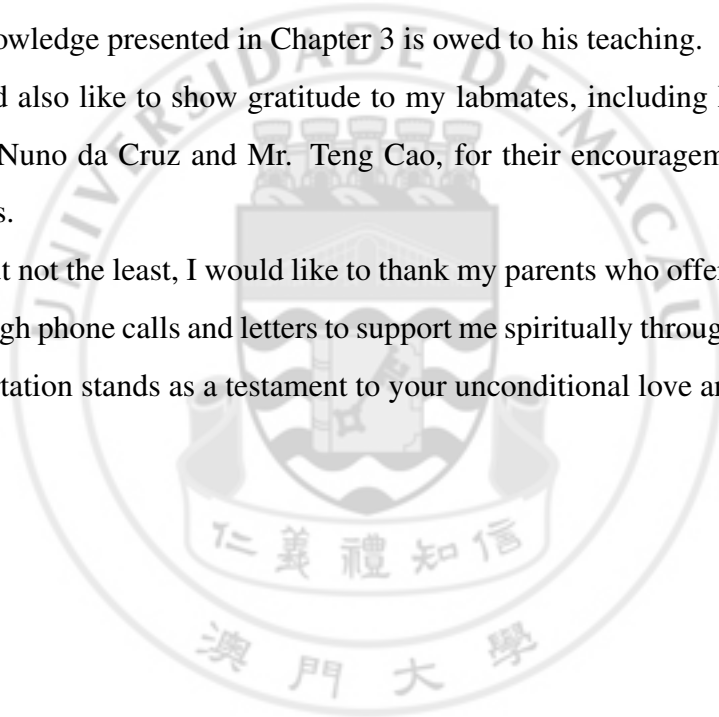
## ACKNOWLEDGMENT

First and foremost, I have to thank my research supervisor, Dr. Feng Wan. Without his assistance and dedicated involvement in every step throughout the process, this project would have never been accomplished. I would like to thank you very much for your support and understanding over these past four years.

Besides my supervisor, I would like to thank Prof. Tao Qian for his patience, enthusiasm, and immense knowledge. He was very patient with my knowledge gaps in the adaptive Fourier decomposition method and pointed out my mistakes about this method. Lots of knowledge presented in Chapter 3 is owed to his teaching.

I would also like to show gratitude to my labmates, including Mr. Chiman Wong, Mr. Janir Nuno da Cruz and Mr. Teng Cao, for their encouragement, comments and discussions.

Last but not the least, I would like to thank my parents who offered their encouragement through phone calls and letters to support me spiritually throughout last four years. This dissertation stands as a testament to your unconditional love and encouragement.



## CONTENTS

<b>1</b>	<b>INTRODUCTION</b>	<b>9</b>
<b>2</b>	<b>BACKGROUND AND LITERATURE REVIEW</b>	<b>12</b>
2.1	FOURIER TRANSFORM . . . . .	12
2.1.1	INTRODUCTION TO THE FOURIER TRANSFORM . . . . .	12
2.1.2	ECG DENOISING BASED ON THE FOURIER TRANSFORM . .	15
2.2	WAVELET TRANSFORM . . . . .	17
2.2.1	INTRODUCTION TO THE WAVELET TRANSFORM . . . . .	17
2.2.2	ECG DENOISING BASED ON THE WAVELET TRANSFORM . . .	20
2.3	EMPIRICAL MODE DECOMPOSITION . . . . .	24
2.3.1	INTRODUCTION TO THE EMPIRICAL MODE DECOMPOSITION	24
2.3.2	INTRODUCTION TO THE ENSEMBLE EMPIRICAL MODE DE- COMPOSITION . . . . .	27
2.3.3	ECG SIGNAL DENOISING BASED ON THE EMD AND THE EEMD . . . . .	30
<b>3</b>	<b>ADAPTIVE FOURIER DECOMPOSITION</b>	<b>34</b>
3.1	INTRODUCTION TO THE ADAPTIVE FOURIER DECOMPOSITION . . .	34
3.2	MATHEMATICAL FOUNDATION OF THE AFD . . . . .	36
3.3	EXAMPLES OF THE AFD . . . . .	37
<b>4</b>	<b>DENOISING BASED ON THE AFD</b>	<b>41</b>
4.1	TECHNIQUE OF THE DENOISING METHOD BASED ON THE AFD . . .	41
4.2	IMPLEMENTATION OF THE DENOISING METHOD BASED ON THE AFD	43
<b>5</b>	<b>SIMULATION RESULTS</b>	<b>46</b>
5.1	ARTIFICIAL ECG SIGNAL . . . . .	46
5.1.1	ADDITIVE GAUSSIAN WHITE NOISE . . . . .	46
5.1.2	COMBINATION REAL NOISE . . . . .	48
5.2	REAL ECG SIGNALS . . . . .	52

5.2.1	ADDITIVE GAUSSIAN WHITE NOISE . . . . .	52
5.2.2	COMBINATION REAL NOISE . . . . .	56
5.3	DISCUSSION . . . . .	57
<b>6</b>	<b>CONCLUSION AND RECOMMENDATIONS FOR FUTURE RESEARCH</b>	<b>63</b>
	<b>REFERENCES</b>	<b>65</b>
	<b>APPENDIX: RELATED PUBLICATIONS</b>	<b>70</b>



## LIST OF FIGURES

2.1	Time domain shape of $x(t) = e^{-3 t-0.5 }$ .	12
2.2	Example of Fourier transform for $x(t) = e^{-3 t-0.5 }$ .	13
2.3	Frequency domain magnitude response plot.	16
2.4	Time-frequency space and resolution cells of wavelet transform.	18
2.5	Four wavelet families.	20
2.6	Threshold signals of the wavelet transform.	22
2.7	Schematic diagram of Hilbert transform.	25
2.8	Calculation steps of EEMD.	29
2.9	ECG denoising method based on the EMD with the spectral flatness.	31
2.10	Tukey window function.	32
2.11	QRS duration of a noisy ECG signal.	33
3.1	$B_n(e^{jt})$ in complex plane.	35
3.2	Real part of Eq. (3.13).	38
3.3	Real part of first six components after AFD.	38
3.4	3D view of first ten AFD results.	39
3.5	Energy of mono-components.	39
4.1	Denoising process based on the AFD with the threshold decomposition level $\epsilon$ .	42
4.2	Flow chart of the denoising method based on the AFD.	44
5.1	Noisy artificial ECG signal with additive Gaussian white noise that makes SNR 5.05dB.	47
5.2	Original artificial ECG signal and filtered result for the additive Gaussian white noise simulation.	47
5.3	Energy ratio of the noisy signals to the reconstructed ECG signal and SNR of the reconstructed ECG signal for different $N$ in the additive Gaussian white noise simulation.	48



5.4	Set of signals for artificial ECG signal simulation of the combination real noise. . . . .	50
5.5	Noisy artificial ECG signal with the combination real noise that makes SNR 14.88dB. . . . .	50
5.6	Original artificial ECG signal and filtered result for the combination real noise simulation. . . . .	51
5.7	Energy ratio of the noisy signal to the reconstructed ECG signal and SNR of the reconstructed ECG signal for different $N$ in the combination real noise simulation. . . . .	52
5.8	Improved SNRs of the filtered signals and corresponding SNRs of the noisy signals for four real signal records: 100, 103, 105 and 119 with additive Gaussian noise. . . . .	52
5.9	Record 103 signal with additive Gaussian white noise that makes the SNR 10dB. . . . .	53
5.10	Original record 103 signal and reconstructed filtered result for the additive Gaussian white noise simulation. . . . .	53
5.11	Record 103 signal with combination real noise that makes the SNR 14dB. . . . .	56
5.12	Original 103 signal and reconstructed filtered result for the combination real noise simulation. . . . .	56
5.13	Optimal decomposition levels for different frequencies of original single sinusoidal signals and SNRs of noisy signals. . . . .	61
5.14	Record 203 ECG signal . . . . .	62

## LIST OF TABLES

2.1	Performance comparison of different wavelet families and different thresholds . . . . .	23
2.2	Simulation results of the ECG denoising method based on the EMD with the spectral flatness . . . . .	32
3.1	Denoising results of four special shape signals based on the AFD . . . .	40
5.1	Performance (SNR) comparison between filtered results based on the wavelet transform and the AFD for the additive Gaussian white noise simulation . . . . .	54
5.2	Performance (MSE) comparison between filtered results based on the EMD, the EEMD and the AFD for the additive Gaussian white noise simulation . . . . .	55
5.3	Performance (SNR) comparison between filtered results based on the EMD, the wavelet transform and the AFD for the combination real noise simulation . . . . .	57
5.4	Performance (MSE) under different decomposition level $N$ for additive Gaussian white noise . . . . .	58
5.5	Performance (SNR) under different decomposition level $N$ for the combination real noise . . . . .	59

## LIST OF SYMBOLS

$f$	Frequency
$\omega$	Angular frequency
$d_j$	$j$ -th detailed coefficient of the wavelet transform
$T$	Threshold of the wavelet transform
$r_N$	Remainder of the empirical mode decomposition at the decomposition level $N$
$H(x)(t)$	Hilbert transform of $x(t)$
SD	Standard deviation
$w(t)$	white noise signal
SNR	Signal-to-noise ratio
SNR <sub>e</sub>	Estimated SNR of the corresponding noisy signal
FT	Spectral flatness
$\Phi(t)$	Window function
$\mathbb{D}$	Unit disc
$\mathbb{C}$	Complex plane
$\mathbb{R}$	Real line
$\mathbb{R}^+$	Positive real line
$H^2(\partial\mathbb{D})$	Hardy space
$L^2(\partial\mathbb{D})$	Laplace space
$R_N$	Standard remainder of the adaptive Fourier decomposition at the decomposition level $N$
$G_n$	Reduced remainder of the adaptive Fourier decomposition at the decomposition level $n$
$B_n$	Rational function in the Takenaka-Malmquist system
$e_{\{a_n\}}$	Evaluator at $a_n$ of the adaptive Fourier decomposition
$n(t)$	Noise signal

## CHAPTER I INTRODUCTION

The adaptive Fourier decomposition, also called AFD, is a novel signal decomposition method proposed by Qian et al. It offers decompositions of signals into basic pieces that only contain positive frequencies by using adaptive basis functions [30]. Moreover, the AFD decomposes signals based on their energy distributions. Therefore, its decomposition components not only have a good convergence property but also follow the sequential extraction of the energy starting from the high-energy mode to the low-energy mode.

According to this characteristic of the AFD, it is very suitable for some noisy signals whose corresponding pure signals and noise have energy differences to do the denoising process. The electrocardiogram (ECG) signals belongs to this kind of signals. Normally, a measurement ECG signal is weak and contain extraneous signals from the muscles, lungs and the internal electronics of the recording devices [11]. Although some linear and nonlinear denoising methods of ECG signals have been proposed, they all have some problems which may damage original signals or make them unpractical.

The Fourier transform is a traditional signal processing method. It transfers signals from their time domain to their frequency domain. There are many kinds of filters based on the Fourier transform method. For these filters, they reconstruct the original signal by using their corresponding frequency components. Although the Fourier transform is very powerful for removing frequency-related noise, it is not very useful when the frequency spectrums of noise and original signals overlap each other. Normally, this problem is very serious for ECG signals. The frequency range of ECG signals is from 0.05Hz to 100Hz. The frequency range of ECG noise is from 0.5Hz to 1000Hz. Therefore, the denoising method based on the Fourier decomposition method may damage original ECG signals. Furthermore, the Fourier transform is only suitable for strictly periodic and stationary signals. However, ECG signals usually are non-stationary. Therefore, the Fourier decomposition method is not very suitable for the denoising process of ECG signals. To overcome these drawbacks of the Fourier transform method in the denoising process, the denoising methods based on the wavelet transform were proposed [1, 12, 32, 35, 39]. The wavelet transform decomposes signals

based on a mother wavelet. It considers not only the frequency information but also the time information. Moreover, these wavelet-based denoising method have a good performance for the denoising of the Gaussian white noise. However, this method has two significant problems. First, its decomposition results are related with the choice of the mother wavelet. Different mother wavelets produce different decomposition results, which produces very large difference of filtered results. In addition, it is difficult to find a suitable mother wavelet that can always provide good filtered results. Usually, when the signal is changed, the corresponding mother wavelet also need to be changed, which makes this method unpractical. Second, in practice, the wavelet transform may lead to the oscillation of the reconstructed ECG signal or reduce the amplitude of the ECG waveforms [32], which may damage some useful information of the original ECG signals. To solve these two problems of the wavelet transform, some other papers propose the denoising methods based on the empirical mode decomposition (EMD) [8,41]. The main technique of the denoising method based on the EMD is to decompose the noisy signal into some intrinsic mode functions (IMFs), remove IMFs that contain most noise and then reconstruct the signal with remaining IMFs. Since the decomposition is based on the local characteristics of the data, the basis function of the EMD can be derived adaptively. In addition, the EMD has good localization properties [29]. Therefore, the oscillation problem does not exist in its reconstructed signals. However, this method does not have an explicit mathematical explanation. In practice, it is difficult to understand its decomposition components and interpret its decomposition results. Therefore, it is difficult to define a threshold of the decomposition level of the EMD. Usually, the Fourier transform still needs to be applied analyzing the decomposition components of the EMD which makes the EMD process not meaningful. Moreover, in some cases, analytic phase functions of IMFs are not monotone [36]. In other words, a physically meaningful analytic instantaneous frequency of IMFs cannot be defined in generally. In addition, IMFs may have negative phase derivatives in practice, which will effect the analysis of the decomposition results based on the EMD and the threshold judgment [29].

Comparing with these three classical signal processing methods, the AFD mainly has three major advantages. First, the basis functions are fixed to signals adaptively. Therefore, we don't need to worry about the problem of choosing basis functions. Sec-

ond, it has a rigorous mathematical foundation, which makes finding physical meaning of its decomposition components easy. Third, all decomposition results are mono-components whose analytic phase derivatives are non-negative. In other words, it allows application-related mathematical analysis of signals. Since the AFD has these advantages, in this report, the AFD is applied implementing a denoising process for the ECG signals. The technique of the AFD-based denoising process is to stop the recursive AFD process when enough mono-components have been obtained and reconstruct the filtered result using these mono-components. This report will mainly focus on how to find the judgment to determine if enough mono-components have been obtained and show the effectiveness of the AFD in the ECG denoising field. This method is demonstrated through an artificial ECG signal generated by a ECG model [22] and real ECG signals from the MIT-BIH Arrhythmia Database [14,23]. Three different types of noise, included additive Gaussian white noise, muscle and electrode motion artifacts, is added. For the simulation results, four types of denoising methods based on the Fourier transform, the wavelet transform, the EMD and the ensemble empirical mode decomposition (EEMD) are applied comparing with the proposed method to show that the proposed AFD-based denoising method is a promising tool for ECG signal denoising.

This report is structured as follows. In Chapter 2, the existing signal processing methods and their corresponding technique of the signal denoising methods are reviewed. In Chapter 3, a brief introduction to the AFD method included its principle and mathematical foundation proposed by Qian et al. is given. In Chapter 4, I work on how to use the AFD to do the denoising process. a judgment to make the AFD practical in the signal denoising process is defined. In addition, how to implement it is introduced. In Chapter 5, several simulation results of the proposed AFD-based signal denoising method are shown by using two types of ECG signals with three types of noise. Moreover, the filtered results of other denoising methods based on the low-pass filter, the wavelet-based, the EMD-based and the EEMD-based denoising methods are applied comparing with the filtered results of the AFD-based denoising method. Then, according to these simulation results, some small problems of this proposed denoising method can be found. These problems and how to solve them are also discussed in Chapter 5. Finally, in Chapter 6, a conclusion and discussion about the further directions of the application of the AFD are given.

## CHAPTER II BACKGROUND AND LITERATURE REVIEW

### 2.1 FOURIER TRANSFORM

#### 2.1.1 INTRODUCTION TO THE FOURIER TRANSFORM

Fourier transform is a traditional mathematical transform which is employed to transfer a signal from its time domain to its frequency domain. It decomposes signals to a linear combination of several trigonometric functions as shown in Eq. (2.1) [25]. Fig. 2.2 shows the principle of Fourier transform more clearly. It is an example of Fourier transform for  $x(t) = e^{-3|t-0.5|}$  shown in Fig. 2.1. Although there should be a sinusoidal wave in every frequency from  $-\infty$  to  $\infty$ , only several waves are shown in Fig. 2.2 to make sure that shapes of components can be seen clearly. For different components, they are all sinusoidal waves which don't have phase difference. The only differences are their frequencies and amplitudes. Therefore, it is easy to get the frequency point of view for a strictly periodic and stationary signal by using the Fourier transform.

$$x(t) = \sum_{k=-\infty}^{\infty} a_k [\cos(2\pi kft) + j \sin(2\pi kft)] \quad (2.1)$$

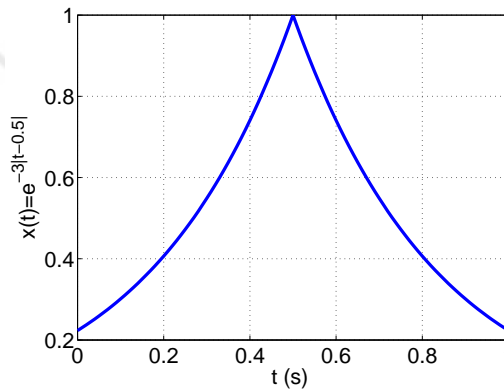


**Fig. 2.1** Time domain shape of  $x(t) = e^{-3|t-0.5|}$ .

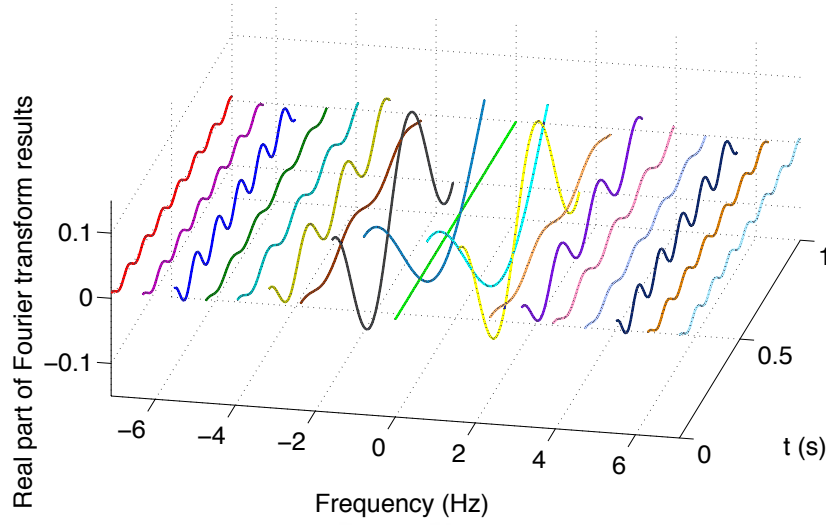


**Fig. 2.2** Example of Fourier transform for  $x(t) = e^{-3|t-0.5|}$ .

For Fourier transform, signals are considered as a linear combination of complex exponential functions as shown in Eq. (2.2) [25].  $X(j\omega)$  is the Fourier transform of  $x(t)$ . Eq. (2.3) is called Fourier transform or Fourier integral of  $x(t)$ . It extracts spectrum information from the signal. Eq. (2.2) is called inverse Fourier transform of  $X(j\omega)$ . It synthesizes the time-domain signal from the spectral information [25, 31]. Eq. (2.2) and Eq. (2.3) are called Fourier transform pair. By using this transform pair, it is easy to transfer signals from time domain to frequency domain or from frequency domain to time domain.

$$x(t) = \frac{1}{2\pi} \int_{-\infty}^{\infty} X(j\omega) e^{j\omega t} d\omega \quad (2.2)$$

$$X(j\omega) = \int_{-\infty}^{\infty} x(t) e^{-j\omega t} dt \quad (2.3)$$

From the Fourier transform, we can get the information of magnitudes and phases for different frequencies at the same time. The magnitude determines the amplitude of each complex exponential function required to reconstructed the desired signal  $x(t)$  from its Fourier transform. It determined as

$$|X(j\omega)| = \sqrt{\text{Re}\{X(j\omega)\}^2 + \text{Im}\{X(j\omega)\}^2}. \quad (2.4)$$

The phase determine the time shift of each decomposition component relative to refer-



ence of time zero. It can be shown as

$$\theta(\omega) = \tan^{-1} \left( \frac{\text{Im}\{X(j\omega)\}}{\text{Re}\{X(j\omega)\}} \right). \quad (2.5)$$

As we can see from this introduction to the Fourier transform, the Fourier transform is able to provide accurate frequency information including the amplitude and the phase information. In addition, it contains several properties that help simplify function domain transformations [11]:

#### (1) Linearity

The Fourier transform is a linear operator. Therefore, for any constants  $a_1$  and  $a_2$ ,

$$F\{a_1x_1(t) + a_2x_2(t)\} = a_1X_1(j\omega) + a_2X_2(j\omega). \quad (2.6)$$

This property demonstrates that the scaling and superposition properties defined for a linear system also hold for the Fourier transform.

#### (2) Time Shifting

If  $x_1(t - t_0)$  is a signal in the time domain, its corresponding Fourier transform can be shown as

$$F\{x_1(t - t_0)\} = X(j\omega) \cdot e^{-j\omega t_0}. \quad (2.7)$$

#### (3) Frequency Shifting

If  $X_1(\omega - \omega_0)$  is the Fourier transform of a signal, its corresponding inverse Fourier transform is

$$F^{-1}\{X_1(\omega - \omega_0)\} = x(t) \cdot e^{-j\omega_0 t}. \quad (2.8)$$

#### (4) Convolution Theorem

The convolution between two signals  $x_1(t)$  and  $x_2(t)$  in the time domain is defined as

$$x_1(t) * x_2(t) = \int_{-\infty}^{\infty} x_1(t)x_2(t - \tau)d\tau \quad (2.9)$$

where  $*$  is the convolution operator. Its corresponding equivalent expression in the frequency domain is

$$C(j\omega) = F\{x_1(t) * x_2(t)\} = X_1(j\omega) \cdot X_2(j\omega) \quad (2.10)$$

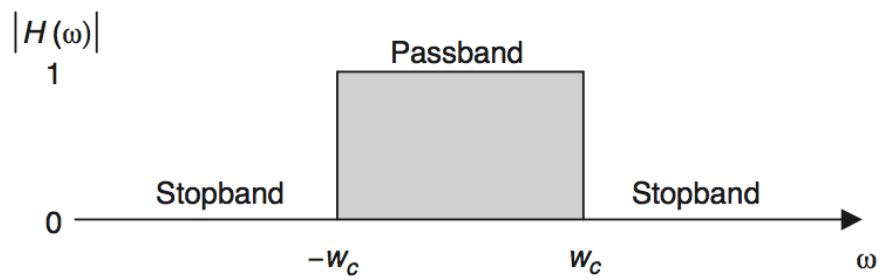
According to these properties, Fourier transform is easy to be implemented for different kinds of situations. However, it also has three serious drawbacks. First, after the Fourier transform, the time information of the original signal is lost. Sometimes, the time information for biosignals is very important. Second, the convergence property is bad. Whenever the Fourier transform is calculated, all frequency domain should be scanned. For most biosignals, they only contain low frequency components. However, the Fourier transform still need to consider high frequency components. Therefore, the Fourier transform converges very slow. In addition, since the Fourier transform considers the whole time domain, it misses the local changes of high-frequency components in the signal [31], which is the third problem of the Fourier transform. For these drawbacks of the Fourier transform, it is not very suitable for the denoising process of biosignals.

#### 2.1.2 ECG DENOISING BASED ON THE FOURIER TRANSFORM

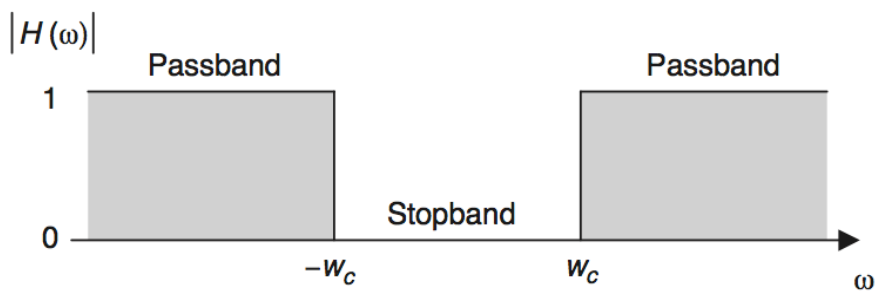
There are some types of filters based on the Fourier transform. According to the characteristics of the Fourier transform, they are all related to the spectrum of signals. The techniques of these filters are almost same. First, the Fourier transform transfers signals from the time domain to the frequency domain. Then, according to the frequency characteristics of original signals and noise, the frequency ranges of noise are removed. Finally, the remaining decomposition components are used to reconstructed the filtered results.

Practically, most filters can be subdivided into three broad classes, according to their modified frequency spectrum of the desired signal. These classes include low-pass filter, high-pass filter and band-pass filters. Low-pass filters work by removing high frequency from a signal while selectively keeping the low frequencies as shown in Fig. 2.3(a) [11]. It allows the low frequencies of the signal to pass through the filter uninterrupted. High-pass filters perform exactly the opposite function of low-pass filters as shown in Fig. 2.3(b) [11]. They selectively pass the high frequencies but remove the low frequencies of the signal. Band-pass filters are like a type of filters between the low-pass filters and high-pass filters. They don't remove the low or high frequencies simply, but remove both high and low frequencies and keep selectively a small band of frequencies as shown in Fig. 2.3(c). The function of band-pass filters can be achieved by combining low-pass filters and high-pass filters. For the band-pass filters, there is a

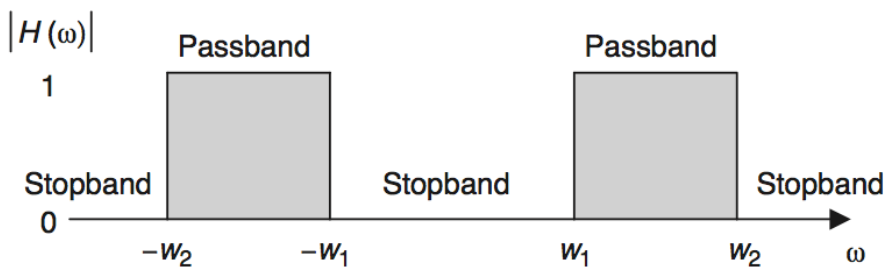
special case. These filters like a inverse of band-pass filters. They normally are called band-stop filters or notch filter as shown in Fig. 2.3(d).



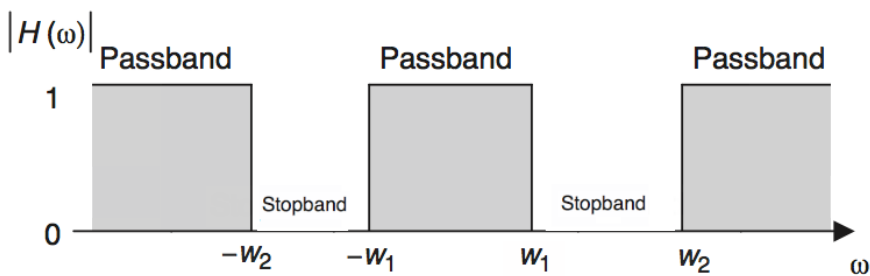
(a) low-pass filter



(b) high-pass filter



(c) band-pass filter



(d) band-stop filter

**Fig. 2.3** Frequency domain magnitude response plot.

For ECG signals, there are mainly three types of noise that are corresponding to these three types of filters. Power line noise is a very common noise whose frequency is 50Hz or 60Hz [11]. Normally, its amplitude is 50% of the maximum value of the ECG signal. According to the frequency range of this type of noise, band-pass filters can be used to remove it. Another type of noise is the electrode contact noise. This type of noise normally causes the baseline drift of the ECG signals. The frequency range of the electrode contact noise usually is smaller than 0.5Hz. High-pass filters with cut-off frequency at 0.5Hz can be used to remove this type of noise [11]. The third type of noise is the muscle artifact, also called EMD noise. The frequency range is from 20Hz to 1000Hz [11]. Low-pass filters with 40Hz cut-off frequency can be used to remove this type of noise.

Although these filters based on the Fourier transform can remove noise from ECG signals, they also damage original signals' information. The frequency range of ECG signals usually is from 0.05Hz to 100Hz [11]. Therefore, there are overlapped frequency ranges between the ECG signals and noise. For filters based on the Fourier transform, they cut off selected frequency components directly. However, these selected frequency ranges also contain some useful information from the original ECG signals. This is a very serious problem of filters based on the Fourier transform.

## 2.2 WAVELET TRANSFORM

### 2.2.1 INTRODUCTION TO THE WAVELET TRANSFORM

To overcome drawbacks of filters based on the Fourier transform, the wavelet transform was proposed. The wavelet transform is similar with the Fourier transform. It is also a method to decompose original signal to some basis components. It isn't based on sinusoidal waves but based on wavelets, which are small waves of varying frequency and limited duration. The most important aspect of the wavelet basis is that all wavelet functions are constructed from a single mother wavelet. This wavelet is a small wave or a pulse [31]. It can transfer a continuous function into a highly redundant function [13]. Although wavelet transform and short time Fourier transform all can do time-frequency analysis, they are different. The most important feature of the wavelet transform is that it analyzes different frequency components of a signal with different resolutions.

If there is a function  $f(\frac{t}{a})$  for any scale  $a$ , a function with lower frequency will be

obtained which is able to describe slowly changing signals when  $a > 1$ , and a function with higher frequency will be obtained that can detect fast changing signals. In other words, the scale is inversely proportional to the frequency. For the wavelet transform, the resolution of frequencies  $\sigma_\omega$  and the resolution of time  $\sigma_T$  are not same. Therefore, good resolution of frequency or time in a space of time can be obtained as shown in Fig. 2.4.

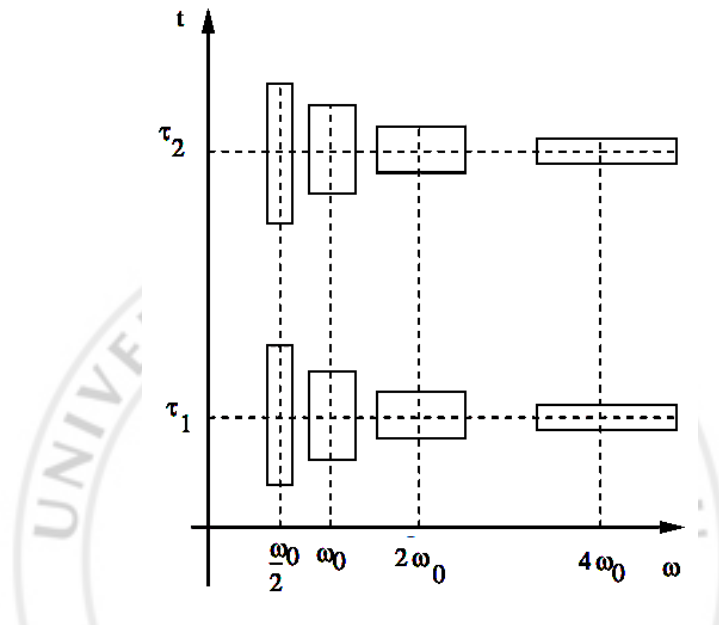
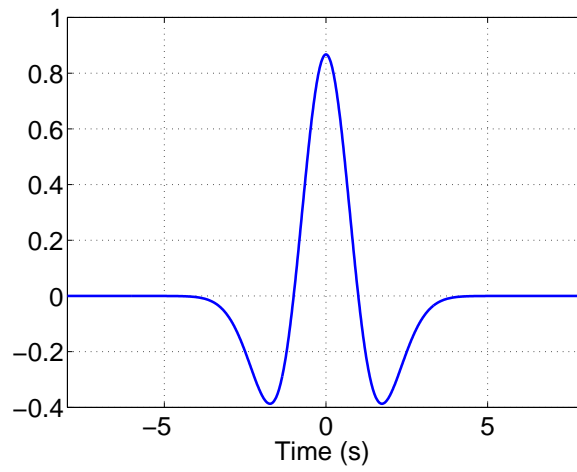
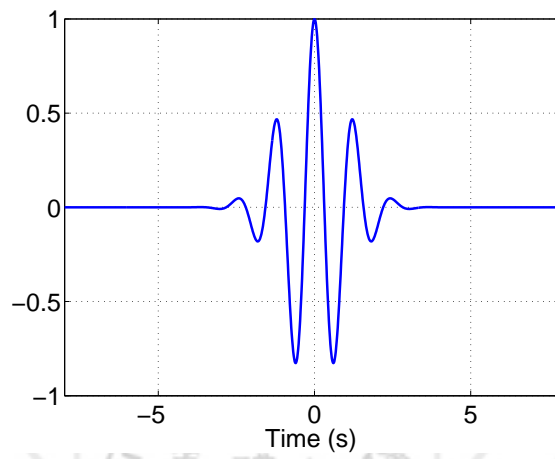


**Fig. 2.4** Time-frequency space and resolution cells of wavelet transform.

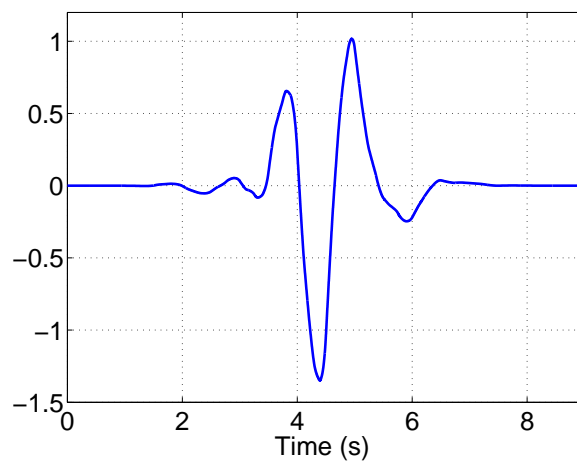
Wavelet functions aren't the same as sinusoidal waves. They aren't only localized in frequency but also localized in time. But wavelets functions only can offer the good time resolution or the good frequency resolution. There are several wavelet families. Different wavelet families has its own character shape and fixed interval of time. Fig. 2.5 shows 4 wavelet families as examples. The number of wavelet families is much larger than 4.



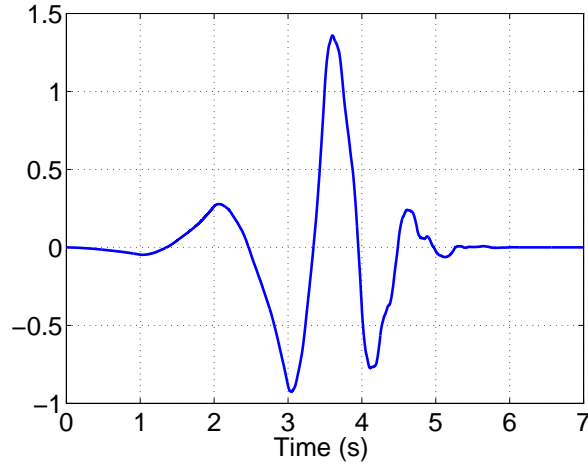
(a) Mexican-hat wavelet



(b) Morlet wavelet



(c) Symlets wavelet



(d) Daubechies wavelet

**Fig. 2.5** Four wavelet families.

A wavelet can be defined by the scale and shift parameters  $a$  and  $b$ ,

$$\phi_{ab}(t) = \frac{1}{\sqrt{a}} \phi\left(\frac{t-b}{a}\right) \quad (2.11)$$

while the wavelet transform is given by the inner product

$$W(a, b) = \int_{-\infty}^{\infty} \phi_{ab}(t) f^*(t) dt \quad (2.12)$$

with  $a \in \mathbb{R}^+$ ,  $b \in \mathbb{R}$ . The wavelet transform defines an  $L^2(\mathbb{R}) \rightarrow L^2(\mathbb{R}^2)$  mapping which has a better time-frequency location than the short time Fourier transform [31].

### 2.2.2 ECG DENOISING BASED ON THE WAVELET TRANSFORM

The technique of the filters based on the wavelet transform is also similar with the filters based on the Fourier transform. First, the wavelet transform decompose signals to decomposition components. Then some decomposition components which contains noise are removed. Finally, the remaining decomposition components are used to reconstruct the filtered results. Since the decomposition components of the wavelet transform are related with the mother wavelet. Different mother wavelet produce different decomposition components and different filtered results. Therefore, choosing a suitable mother wavelet is very important. However, it is not easy. For ECG signals, the shapes and characteristics of signals from different records may different. Therefore, it is difficult to choose a appropriate mother wavelet once and for all. Most papers use the Daubechies

wavelets and Symlet wavelets as the mother wavelet families [1, 12, 32, 35, 39]. Another problems of filters based on the wavelet transform is the threshold. How to define or choose a suitable threshold to make sure that most original signal can be reconstructed is also very important. There are mainly two kinds of classical thresholds for the wavelet transform [1, 32]: hard threshold and soft threshold. Beside these two kinds of threshold, some papers provide improved threshold. [32] provides a kind of improved threshold which can provide a better filtered performance for ECG signals. [35] provides a kind of adaptive threshold whose parameters can fix to the ECG signals adaptively. Although the techniques of different threshold are different, they are all based on the hard threshold and soft threshold. Therefore, these two basic thresholds are introduced:

(1) Hard threshold

For the hard threshold, all selected decomposition components are removed totally. Remained decomposition components also are used totally. Fig. 2.6(b) shows the idea of the hard threshold. Eq. (2.13) shows the hard threshold of the wavelet transform where  $d_j$  and  $T_j$  are the detailed coefficients obtained by the wavelet transform and the threshold respectively [32].

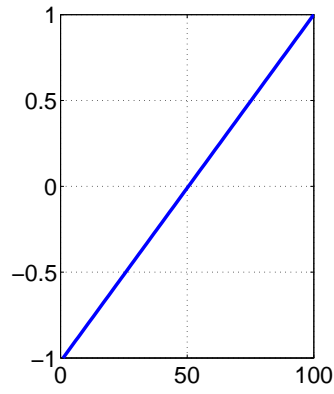
$$\hat{d}_j = \begin{cases} d_j & |d_j| > T_j \\ 0 & |d_j| \leq T_j \end{cases} \quad (2.13)$$

(2) Soft threshold

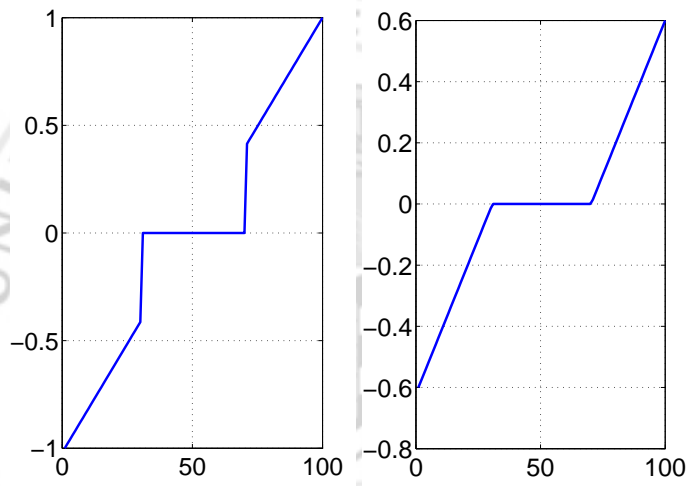
For the soft threshold, only part of selected decomposition components are removed. Fig. 2.6(c) shows the idea of the soft threshold. Eq. (2.14) shows the soft threshold of the wavelet transform where  $d_j$  and  $T_j$  are the detailed coefficients obtained by the wavelet transform and the threshold respectively [32].

$$\hat{d}_j = \begin{cases} \text{sgn}(d_j) (|d_j| - T_j) & |d_j| > T_j \\ 0 & |d_j| \leq T_j \end{cases} \quad (2.14)$$





(a) original signal



(b) hard threshold signal

(c) soft threshold signal

**Fig. 2.6** Threshold signals of the wavelet transform.

**Table 2.1** Performance comparison of different wavelet families and different thresholds

Daubechies wavelets			Symlet wavelets		
Wavelet	Threshold	SNR	Wavelet	Threshold	SNR
db2	Hard	14.4833	sym2	Hard	14.2894
	Soft	14.8544		Soft	14.5527
db3	Hard	14.4590	sym3	Hard	14.7639
	Soft	14.7818		Soft	14.7639
db4	Hard	14.4104	sym4	Hard	14.3775
	Soft	14.7232		Soft	14.6844
db5	Hard	14.5275	sym5	Hard	14.4386
	Soft	14.9290		Soft	14.6972
db6	Hard	14.3753	sym6	Hard	14.3517
	Soft	14.7343		Soft	14.6959
db7	Hard	14.4861	sym7	Hard	14.7601
	Soft	14.8007		Soft	14.7601
db8	Hard	14.3846	sym8	Hard	14.3713
	Soft	14.6935		Soft	14.6522

There is a summary of these two kinds of thresholds and two kinds of mother wavelet families: Daubechies wavelets and Symlet wavelets as shown in Table 2.1 [1,32]. This table shows the signal-to-noise ratio (SNR) of filtered ECG signals' results for different wavelet families and different thresholds. It can be seen that the soft threshold almost can provide a better performance than the hard threshold. However, it is difficult to find which wavelet can provide stable good performances for ECG signals. Most of the time, the Daubechies wavelets can provide better performances.

From this introduction, it can be seen that the most serious problem of the wavelet transform is how to choose a suitable wavelet for its signal decomposition. Since its basis functions can fix to signals adaptively, users need to choose them by their experience, which makes this method not practical. Although the wavelet transform overcomes some drawbacks of the Fourier transform, it still not very suitable for ECG signal denoising.

## 2.3 EMPIRICAL MODE DECOMPOSITION

### 2.3.1 INTRODUCTION TO THE EMPIRICAL MODE DECOMPOSITION

The empirical mode decomposition, also called EMD, is a method to decompose any unstable and nonlinear data set into a finite and small number of ‘intrinsic mode functions’, also called IMFs, that admit well-behaved Hilbert transforms [16]. The original signal can be shown in Eq. (2.15) where  $c_j(t)$  and  $r_N(t)$  are the  $j$ th order IMF and the residual signal [37].

$$s(t) = \sum_{j=1}^N c_j(t) + r_N(t) \quad (2.15)$$

As last sections discussed, Fourier transform and wavelet transform have some disadvantages. For Fourier transform, although it can transfer signals from time domain to frequency domain, it has many disadvantages. It requires that the input must be stable and converge signal. But normally, actual signals are not stable and converge. And since it use the linear combination of trigonometric functions, the energy will spread to whole frequency spectrum which has two drawbacks. First, meaningless negative frequency will be generated. Second, it is difficult for electrical devices to analyze its infinite results. The time information also is lost. Although STFT can save time information, the fix length of windows makes the time resolution and frequency resolution bad. For wavelet transform, it use a wavelet to scan the signal with different window length to overcome the drawback of STFT but the fixed type of wavelets makes choosing a suitable kind of wavelets difficult.

Although EMD is almost similar to the wavelet transform, EMD doesn’t need to choose a basis function before analyzing a data sequence. The basis function will be obtained in the analysis process [16]. Therefore, the basis function will be fixed to the original data automatically. It overcomes the disadvantage of the wavelet transform.

The decomposed results of EMD is some IMFs. They are some signals which satisfied the following two conditions:

- (1) In the whole data set, the number of extrema and the number of zero crossing must either equal or differ at most by one;
- (2) At any point, the mean value of the envelope defined by the local maximum and the

envelope defined by the local minimum is zero.

According to the above two conditions, IMFs are sinusoidal-like waveforms whose amplitudes and phases are changed in different time. Therefore, Eq. (2.16) can be used to present IMFs [16]. Notice that the frequencies of IMFs should be always positive. And IMFs are all converged. Then it is possible to use Hilbert transform to analysis results of EMD. The Hilbert transform is an LTI operator which takes a function  $u(t)$  and produces a function  $H(u)(t)$  with the same domain [15]. The schematic diagram shown in Fig. 2.7 shows the process of Hilbert transform where  $h(t) = \frac{1}{\pi t}$ .

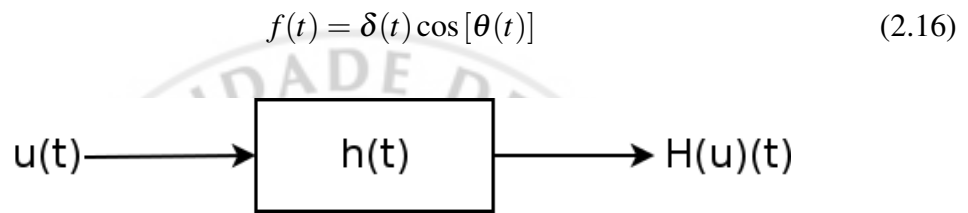


**Fig. 2.7** Schematic diagram of Hilbert transform.

Since the Hilbert transform can be seen as a LTI system, the convolution can be used to calculate Hilbert transform shown in Eq. (2.17). From Eq. (2.17), we can find that Hilbert transform can not be used to analysis all signals. It only can be used to analyze signals which are converged. This is the reason why EMD is needed to decompose signals to IMFs. There are two properties of Hilbert transform shown in Eq. (2.18) and Eq. (2.19). Combining these two properties and Eq. (2.16), it is easy to find that Hilbert transform can be used to analyze instantaneous phase of IMFs by using Eq. (2.20) which provides a way to get the instantaneous frequency.

$$H(u)(t) = h(t) * u(t) = \frac{1}{\pi} \int_{-\infty}^{\infty} \frac{u(\tau)}{t - \tau} d\tau \quad (2.17)$$

$$H(\sin(t)) = -\cos(t) \quad (2.18)$$

$$H(\cos(t)) = \sin(t) \quad (2.19)$$

$$\theta(t) = \tan^{-1} \frac{H(f)(t)}{f(t)} \quad (2.20)$$

To implement the EMD, Hilbert-Huang transform, also called HHT, is proposed. The calculation steps are shown below [16, 40, 43].

- (1) Initialize  $r_0(t) = x(t), j = 1$
- (2) Extract the  $j$ -th IMF:
  - (a) Initialize  $h_0(t) = r_j(t), k = 1$
  - (b) Locate local maximum and minimum of  $h_{k-1}(t)$
  - (c) Cubic spline interpolation to define upper and lower envelope of  $h_{k-1}(t)$
  - (d) Calculate mean  $m_{k-1}(t)$  from upper and lower envelope of  $h_{k-1}(t)$
  - (e) Define  $h_k(t) = h_{k-1}(t) - m_{k-1}(t)$
  - (f) If stopping criteria are satisfied then  $h_j(t) = h_k(t)$  else go to 2.(b) with  $k = k + 1$
- (3) Define  $r_j(t) = r_{j-1}(t) - h_j(t)$
- (4) If  $r_j(t)$  still has at least two extrema then go to 2.(a) with  $j = j + 1$  else the EMD is finished.
- (5)  $r_j(t)$  is the residue of  $x(t)$

From steps, we can find that this method is for continuous signals. But in practical case, discrete signals are actually to be analyzed. For a discrete data sequence, there are two problems which are not mentioned clearly. First is how to define the local extrema. Second is how to adjust whether a signal is an IMF.

For the first problem, the difficulty is to find locations of extrema values. There are two ways to define extrema values for discrete data sequences:

- (1) If a point is satisfied Eq. (2.21), it is the local maximum. If a point is satisfied Eq. (2.22), it is the local minimum. But there are two special cases. First,  $x[n-1] = x[n]$ , and they are all local maximum or local minimum. Normally, the center point will be used. Second, boundary points can not be used in Eq. (2.21) and Eq. (2.22). In most cases, there are two ways to deal with boundary points. First, let them become extrema values directly. Second, copy a part of original data sequence

to boundary to extend original data set. Then use Eq. (2.21) and Eq. (2.22) to determine boundary points.

$$\begin{cases} x[n-1] < x[n] \\ x[n+1] < x[n] \end{cases} \quad (2.21)$$

$$\begin{cases} x[n-1] > x[n] \\ x[n+1] > x[n] \end{cases} \quad (2.22)$$

- (2) The data sequence comes from the sampling process of the original continuous signal. The second way is to recover the data sequence to original continuous signal. Then find extrema points of the continuous signal. This way is very complex but accurate.

For the second problems, there are also two methods [16]:

- (1) According to the definition of IMF, if  $h_k(t)$  satisfied the definition of IMF,  $h_k(t)$  is IMF. Since numbers of extrema and zero are difficult to be determined, this method is difficult to be used.
- (2) Calculate  $SD_k$  using Eq. (2.23) [16]. Normally,  $SD_k$  will be in  $0.2 \sim 0.3$  if  $h_k$  is IMF. Therefore, it can be used as the stopping criteria. Although it is easy to be calculated, it is difficult to define the critical value of  $SD_k$ . Different critical value of  $SD_k$  will make different results for the same signal.

$$SD_k = \frac{\sum_{t=0}^T [h_{k-1}(t) - h_k(t)]^2}{\sum_{t=0}^T h_{k-1}^2(t)} \quad (2.23)$$

### 2.3.2 INTRODUCTION TO THE ENSEMBLE EMPIRICAL MODE DECOMPOSITION

For EMD method, it has a problem – “Mode mixing” problem. This problem mainly has two performances [43]:

- (1) Single IMF consists signals of widely disparate scales.
- (2) Different IMF consists a similar scale residing signal.

In other words, different IMFs should contain different frequency part signals and doesn't have the alias with each others but there will be the alias between different IMFs when the mode mixing problem happens. It will decrease physical meanings of IMFs. The ensemble empirical mode decomposition (EEMD) is a method to avoid this problem of EMD method.

The EEMD method is a method which combines the EMD method and the noise-assisted data analysis (NADA) method [7, 18, 43]. In the NADA method, the ensemble mean is used as a powerful approach, where data are collected by separate observations, each of which contains different noise. The observations are the combination between the original data and added white noise as shown in Eq. (3.1) where  $x(t)$  is the original data set,  $w_i(t)$  is the white noise which is different for different observations and  $x_i(t)$  is the new observation data set.

$$x_i(t) = x(t) + w_i(t) \quad (2.24)$$

If the number of the observation is enough, the noise in each trial will be canceled out in mean value of all observations. And the oscillation of each IMFs will also be canceled out after doing the ensemble mean. Therefore, by adding finite noise, the EEMD method eliminated largely the mode mixing problem and preserve physical uniqueness of decomposition.

The calculation processing is very easy to understand as shown in Fig. 2.8.

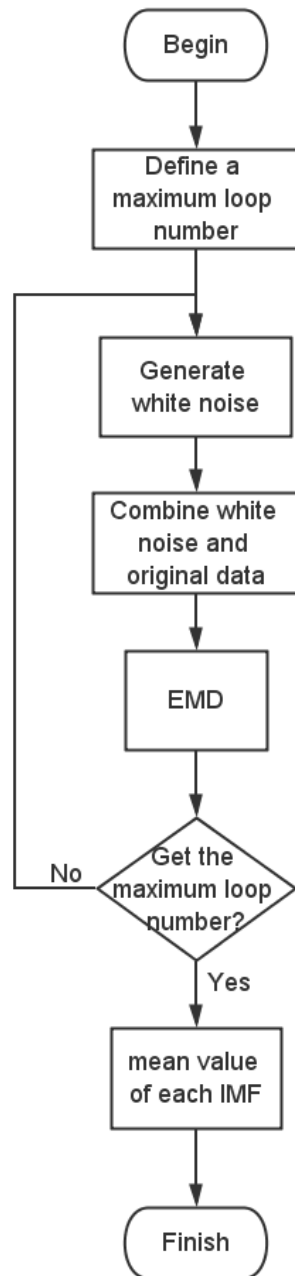


**Fig. 2.8** Calculation steps of EEMD.

Although steps are simple, there are some detail which are needed to be considered:

- (1) The maximum loops number, also called the maximum observations number, should be defined. Since added white noises and oscillations of each IMF need to be canceled out after the ensemble mean, the loops number should be large enough.
- (2) The amplitude of the added white noise should be considered. According to the signal averaging principle, the signal-to-noise ratio (SNR) after averaging is shown



in Eq. (3.2) where  $SNR_{after}$  and  $SNR_{before}$  are signal-to-noise ratios after and before averaging and  $N$  is the number of trials which are used to do the averaging. Since the added noise need to be removed after ensemble mean,  $SNR_{after}$  should be as high as possible. If  $SNR_{before}$  is very small,  $SNR_{after}$  cannot be very high though  $N$  is very large. Therefore, the amplitude of the added white noise also should be controlled.

$$SNR_{after} = \sqrt{N} \cdot SNR_{before} \quad (2.25)$$

- (3) In the simulation, there are two EMD programs which can be used. One is created by G. Rilling [34]. In this program, The boundary situation and the continuous critical points situation are considered. Although the speed is slow, results are good. The other is provided by Zhaohua Wu [42], the author of [43]. This program is used to calculate EEMD directly. In this program, the previous situations are not considered. Except these two situations, other parts are same.

### 2.3.3 ECG SIGNAL DENOISING BASED ON THE EMD AND THE EEMD

The technique of the denoising process based on the EMD and the EEMD is similar with the denoising process based on the wavelet transform. First, the EMD or the EEMD decomposes signals to IMFs. Then some IMFs that include the original signals are selected to reconstruct the filtered results. For the EMD and EEMD, their decomposition results are all adaptive and only contain positive phase derivatives. However, they all don't have a rigorous mathematical functions not only for their procedures but also for their decomposition components. Therefore, it is difficult to find a reasonable and effective method to analysis their decomposition components. Thus it is also difficult to determine which decomposition components should be used to reconstructed the filtered results. According to the characteristics of the IMFs: different IMFs should contain different frequency ranges, some paper use the Fourier transform to analysis IMFs [19, 21]. They use the Fourier transform to get spectrums of IMFs. According to these spectrums, IMFs who contain original signals' frequency spectrum can be found. Then these IMFs can be used to reconstructed the filtered results. Except these methods in which the Fourier transform is used directly, the spectral flatness (FT) factor and

a threshold  $T$  of the FT are used to the ECG denoising [6]. The FT is defined as

$$FT = \frac{\sqrt[L]{\prod_{n=0}^{L-1} H(n)}}{\frac{\sum_{n=0}^{L-1} H(n)}{L}}. \quad (2.26)$$

Normally, the threshold  $T$  is taken as 0.09 [6]. Its corresponding steps of this method is shown in Fig. 2.9. Comparing with the wavelet transform, average simulation results of this method are shown in Table 2.2 [6]. It can be seen that the SNR is improved by using this method. In addition, the results of the EMD is better than the wavelet transform. However, the disadvantage of these methods are also very obvious. The final analysis method is still the Fourier transform. They still are from the frequency point of view to do signal denoising. Therefore, they still contains the disadvantages of the Fourier transform that I have discussed in Section 2.1. Until now, there still are not very reasonable and effective analysis methods for the decomposition components of the EMD and the EEMD. Most of the time, we still need to use our experience to find the useful decomposition components.

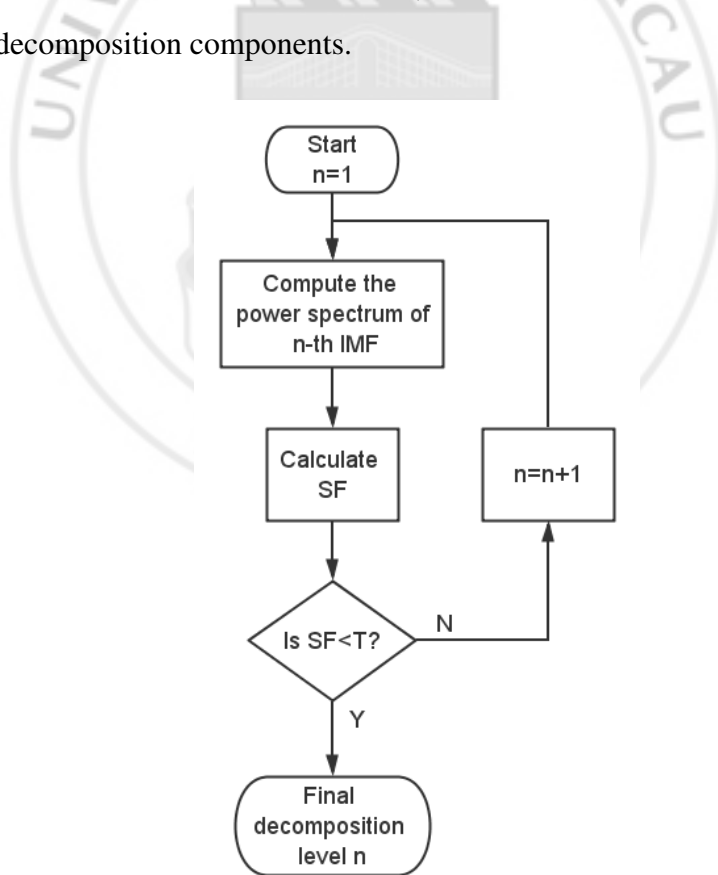


**Fig. 2.9** ECG denoising method based on the EMD with the spectral flatness.

**Table 2.2** Simulation results of the ECG denoising method based on the EMD with the spectral flatness

SNR of noisy signal (dB)	SNR of filtered result (dB)	
	Wavelet transform	EMD
5	8.75	9.92
10	11.96	14.71
15	15.31	18.55

For ECG denoising, the most important thing is to get actual value of the QRS complex. However, sometimes, the filtered results of the EMD cannot reconstructed the QRS range very well. To protect the QRS range, protect windows normally are used in the ECG denoising process based on the EMD [3, 17, 38, 41]. Normally, a Tukey window is used as the protection window shown in Fig. 2.10 [3, 17, 41]. The QRS duration of noisy signals is shown in Fig. 2.11 [3]. After using the protection window, one ECG signal is separated to different parts. For different parts, according to their different SNR, different weight can be added to IMFs to reconstructed a accurate filtered results. The reconstructed result can be shown as

$$\hat{x}(t) = \sum_{i=1}^P \Phi_i(t) c_i(t) + \sum_{i=1}^P a_i \bar{\Phi}_i(t) c_i(t) + \sum_{i=P+1}^N c_i(t) \quad (2.27)$$

where  $0 < a_i < 1$  is the attenuation coefficient as the weight of the non-QRS duration, and  $\Phi_i$  is the protection window.

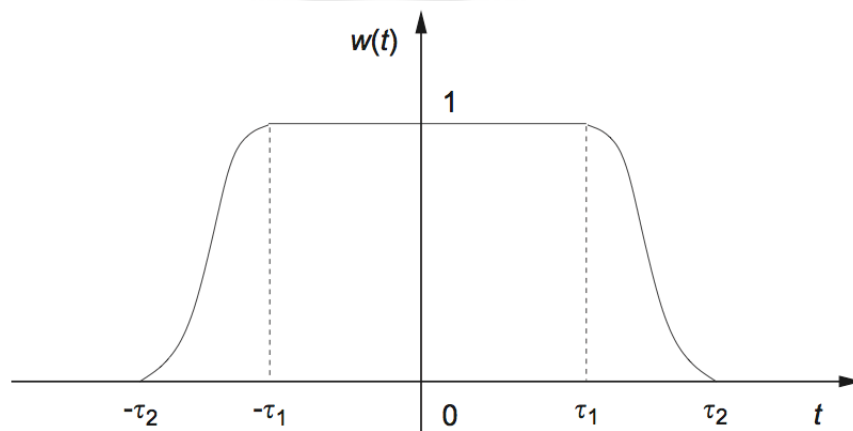


**Fig. 2.10** Tukey window function.

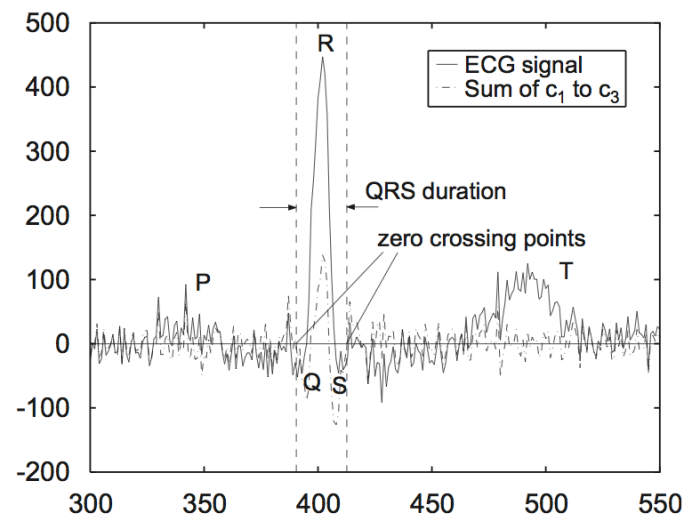


**Fig. 2.11** QRS duration of a noisy ECG signal.

Although the denoising methods based on the EMD overcomes some drawbacks of the denoising methods based on the Fourier transform and the wavelet transform, the EMD doesn't have a rigorous mathematical function which makes the decomposition components of the EMD difficult to be understood and analyzed. Therefore, they are still not very suitable for the ECG denoising.

## CHAPTER III ADAPTIVE FOURIER DECOMPOSITION

### 3.1 INTRODUCTION TO THE ADAPTIVE FOURIER DECOMPOSITION

The adaptive Fourier decomposition, also called AFD, is a novel signal decomposition method proposed by Qian et al. [27, 30]. It involves the adaptive decomposition of a given signal  $G(t)$  that is in  $H^2(\partial\mathbb{D})$  space where  $\mathbb{D} = \{z \in \mathbb{C} : |z| < 1\}$  and  $\mathbb{C}$  is the complex plane into a series of mono-components [27, 30]. After the AFD,  $G(t)$  will be decomposed into a summation of a series of mono-components  $s_n(t)$ 's and a standard remainder  $R_N(t)$  shown in Eq. (3.1) [27, 30]. From Eq. (3.1), it can be seen that signals in  $H^2(\partial\mathbb{D})$  space only have positive frequency. In addition, the decomposition components of the AFD are also only contain positive frequency components. However, in practice, most real signals  $s(t)$ 's are in  $L^2(\partial\mathbb{D})$  space. In other words, according to the Fourier transform, signals in practice contain positive and negative frequency components at the same time. Therefore, it is impossible to reconstruct signals from  $L^2(\partial\mathbb{D})$  space to  $H^2(\partial\mathbb{D})$  space. Thus the relationship shown in Eq. (3.2) where  $f$  and  $f^+$  are signals in  $L^2(\partial\mathbb{D})$  space and  $H^2(\partial\mathbb{D})$  space is used to reconstruct original signals from mono-components [30].

$$G(t) = \sum_{k=0}^{\infty} c_k e^{jkt} = \sum_{n=1}^N s_n(t) + R_N(t), \quad \sum_{k=0}^{\infty} |c_k|^2 < \infty \quad (3.1)$$

$$f = \sum_{k=-\infty}^{\infty} c_k e^{jkt} = 2 \operatorname{Re} \{f^+\} - c_0, \quad \sum_{k=-\infty}^{\infty} |c_k|^2 < \infty \quad (3.2)$$

The AFD use the rational orthogonal system, or the Takenaka-Malmquist system,  $\{B_n\}_{n=1}^{\infty}$ , as its basis functions where

$$B_n(e^{jt}) = \frac{\sqrt{1 - |a_n|^2}}{1 - \bar{a}_n e^{jt}} \prod_{k=1}^{n-1} \frac{e^{jt} - a_k}{1 - \bar{a}_k e^{jt}}, \quad (3.3)$$

$a_n \in \mathbb{D}$ ,  $n = 1, 2, \dots$  [27, 30]. For  $B_n(e^{jt})$ , it has two characteristics. First, in Eq. (3.3),  $\frac{e^{jt} - a_k}{1 - \bar{a}_k e^{jt}}$  is a complex number. In addition, its amplitude is always equal to 1 for any  $e^{jt}$  and  $a_n$ . Therefore,  $B_n(e^{jt})$  can be represented as [27, 28]

$$B_n(e^{jt}) = \rho_n(t) e^{j\phi_n(t)}. \quad (3.4)$$

Second, characteristics of  $B_n(e^{jt})$  are related with  $a_n$ . Different arrays  $[a_1, a_2, \dots, a_n]$  produce different  $B_n(e^{jt})$ . Since the magnitude of  $B_n$  is always one,  $a_n$  mainly decides the phase characteristics. Fig. 3.1 shows  $B_n(e^{jt})$  in the complex plane.  $B_n(e^{jt})$  are the arrows whose start points are the original point, and stop points are in the unit circle. The center point of this unit circle is not always same as the original point.  $a_n$  decides the location of this unit circle. From the phase derivatives of  $B_n(e^{jt})$ , it can be seen that  $B_n(e^{jt})$  are not always mono-components. To make sure that they are mono-components,  $a_1$  must be 0. In addition, comparing Eq. (3.3) and the basis function of the Fourier transform  $e^{jt}$ , it can be found that  $B_n(e^{jt})$  will become the basis function of the Fourier transform if all  $a_n$ 's are equal to 0. Therefore, the Fourier transform can be seen as a special case of the adaptive Fourier decomposition. As I have mentioned in Section 2.1, the most serious problem of the Fourier transform is the bad convergence properties. The adaptive Fourier decomposition solves this problems. Its basis functions fixes signals adaptively and are obtained based on the energy distributions of signals. All mono-components are from high energy to low energy. Moreover, they converge very fast. These characteristics are all decided by  $a_n$ . Therefore, the main purpose of the AFD is to find such kind of array  $\{a_1, a_2, \dots, a_n\}$  that is able to achieve these characteristics.

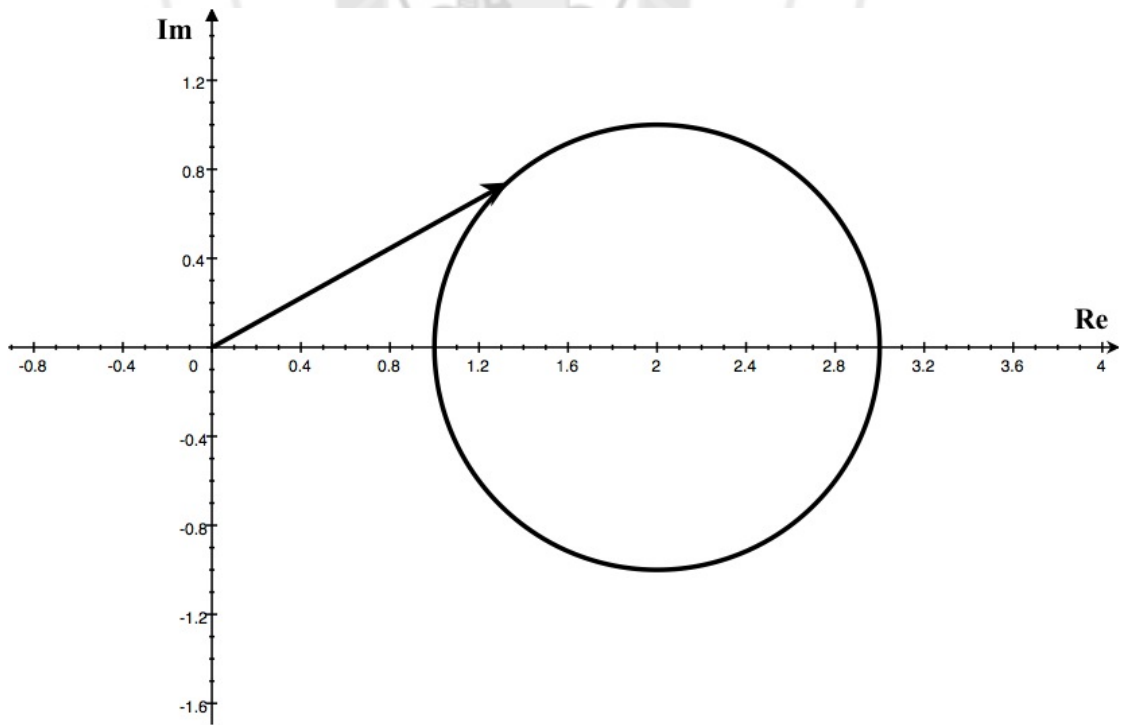


**Fig. 3.1**  $B_n(e^{jt})$  in complex plane.

### 3.2 MATHEMATICAL FOUNDATION OF THE AFD

In the algorithm of the AFD, all mono-components will be found one by one in the energy point of view. The AFD extracts mono-components from the high-energy mode to the low-energy mode sequentially. Since the decomposition components of the AFD must be mono-components first,  $a_1$  needs to be 0 as I have discussed in Section 3.1. Then I will introduce how to make sure that all mono-components converge fast. To find energy relationship easily, reduced remainders  $G_n$ 's are defined by using their corresponding standard remainders  $R_{n-1}$ 's [30]:

$$G_n(e^{jt}) = R_{n-1}(e^{jt}) \prod_{l=1}^{n-1} \frac{1 - \bar{a}_l e^{jt}}{e^{jt} - a_l}. \quad (3.5)$$

Then Eq. (3.1) can be expressed by using reduced remainders  $G_n$ 's:

$$G(t) = \sum_{n=1}^N \langle G_n, e_{\{a_n\}} \rangle B_n(e^{jt}) + G_{N+1}(e^{jt}) \prod_{n=1}^N \frac{e^{jt} - a_n}{1 - \bar{a}_n e^{jt}} \quad (3.6)$$

where  $e_{\{a_n\}}(e^{jt})$  is called the evaluator at  $a_n$  which can be considered as a dictionary consisting of elementary functions [30]:

$$e_{\{a_n\}}(e^{jt}) = \frac{\sqrt{1 - |a_n|^2}}{1 - \bar{a}_n e^{jt}}. \quad (3.7)$$

According to Eq. (3.6), the energy of  $G(t)$  can be calculated by [30]

$$\|G(t)\|^2 = \sum_{n=1}^N |\langle G_n, e_{\{a_n\}} \rangle|^2 + \|G_{N+1}(e^{jt})\|^2. \quad (3.8)$$

To make the energy of the standard remainder  $\|G_{N+1}(e^{jt})\|^2$  minimum, the maximal projection principle shown in Eq. (3.9) is used to find  $a_n$  which can produce the largest  $|\langle G_n, e_{\{a_n\}} \rangle|^2$  for every step  $n$  [30]. After getting the array  $\{a_1, a_2, \dots, a_n\}$ , the main part of the AFD has been finished.

$$a_n = \arg \max \left\{ |\langle G_n, e_{\{a_n\}} \rangle|^2 : a_n \in \mathbb{D} \right\} \quad (3.9)$$

After the decomposition, for given threshold  $\varepsilon > 0$  which sets to have the consecutive maximal sifting processes ceased at the first  $N$  such that

$$\|R_N\|^2 \leq \varepsilon, \quad (3.10)$$

the approximation of the original signal by the summation of the first  $N$  mono-components is [30]

$$G(z) \approx \sum_{n=1}^N \frac{(a - |a_n|^2) G_n(a_n)}{1 - \bar{a}_n e^{jt}} \prod_{l=1}^{n-1} \frac{e^{jt} - a_l}{1 - \bar{a}_n e^{jt}}. \quad (3.11)$$

By using Eq. (3.2), its corresponding function in the  $L^2(\partial\mathbb{D})$  space can be shown as [30]

$$s(e^{jt}) = 2\text{Re} \sum_{n=1}^N \frac{(a - |a_n|^2) G_n(a_n)}{1 - \bar{a}_n e^{jt}} \prod_{l=1}^{n-1} \frac{e^{jt} - a_l}{1 - \bar{a}_n e^{jt}} - c_0 \quad (3.12)$$

From the algorithm, we can see that there is a very large difference between the AFD and traditional decomposition methods. The AFD decomposes signals according to their energy distribution, making the AFD suitable for separating two parts whose frequency ranges overlap each other.

### 3.3 EXAMPLES OF THE AFD

There are examples to show the characteristics of the AFD. The first example is to show the principle of the AFD. The analyzed signal is shown in Eq. (3.13) where  $z = e^{j\omega t}$  and Fig. 3.2. The first six components after the decomposition of AFD is shown in Fig. 3.3. It is difficult to see clearly the result of AFD only from Fig. 3.3. There is a 3D view of the AFD result shown in Fig. 3.4 where the red wave is the original signal.

Fig. 3.5 shows energy of mono-components. As the level  $n$  increase, the energy reduces very fast. In other words, we can use very small components to reconstruct original signal.

$$G(z) = \frac{0.0247z^4 + 0.0355z^3}{(1 - 0.9048z)(1 - 0.3679z)} \quad (3.13)$$



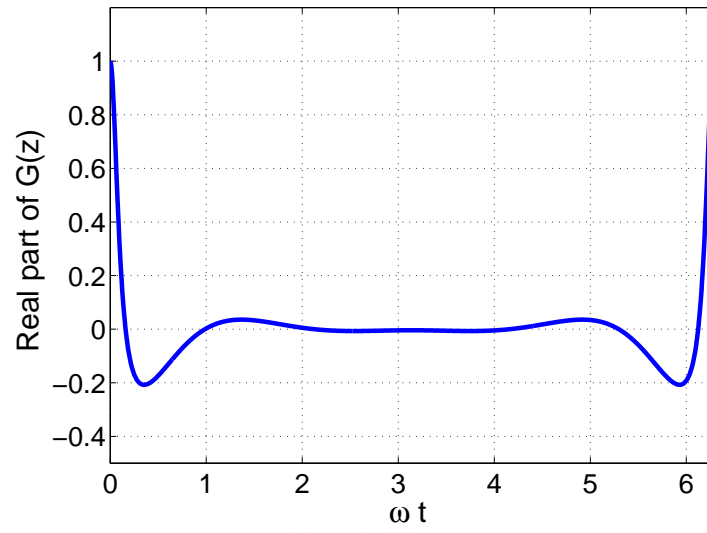


**Fig. 3.2** Real part of Eq. (3.13).

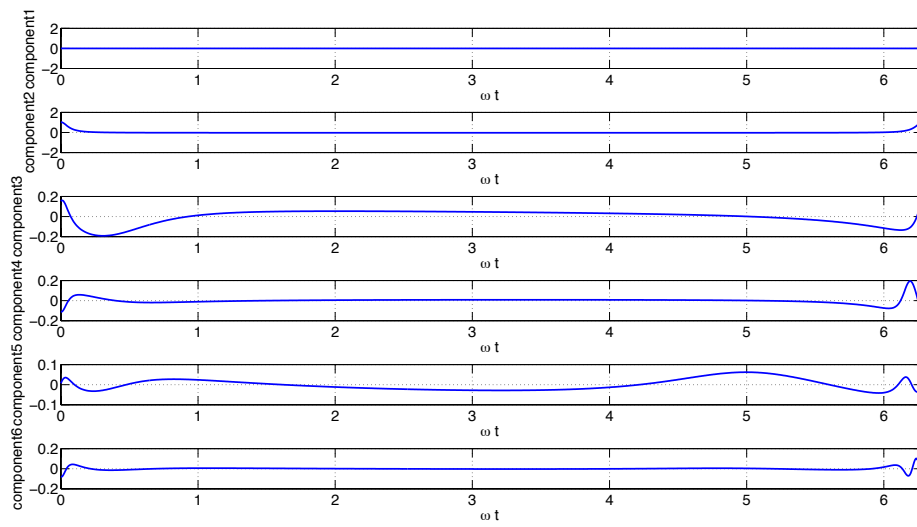


**Fig. 3.3** Real part of first six components after AFD.

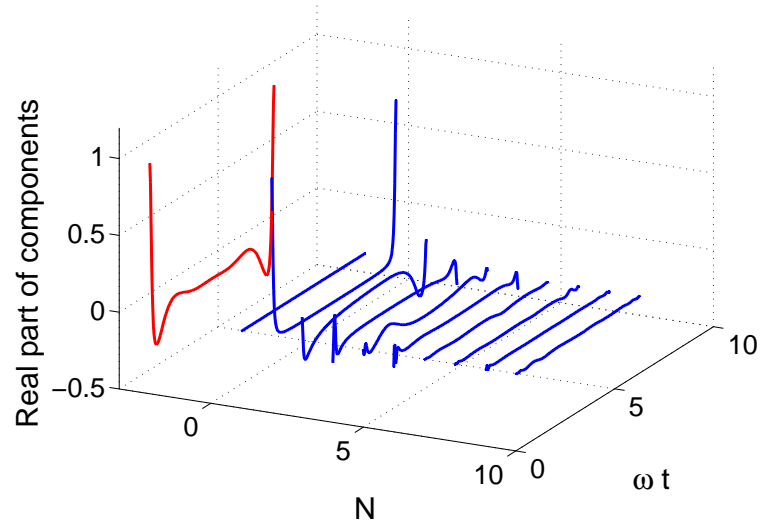


**Fig. 3.4** 3D view of first ten AFD results.

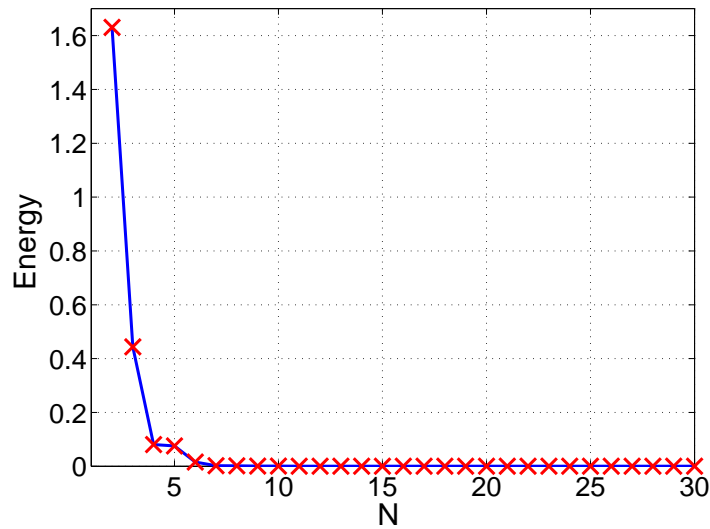


**Fig. 3.5** Energy of mono-components.

To show the effective of the AFD in the denoising process, there are four special waveforms: doppler, blocks, heavysine and bumps with additive Gaussian white noise. Eq. (3.14), Eq. (3.15), Eq. (3.16) and Eq. (3.17) shows these four waveforms: doppler, blocks, heavysine and bumps respectively [10]. For these four signals, the sampling frequency is 2048Hz. SNRs of noisy signals are all 2dB. The wavelet transform and the EMD are also used to do the denoising process of these four signals. The filter results are shown in Table 3.1. From this table, it can be seen that the AFD mostly provides the

best performance in these three methods.

$$f(t) = \sqrt{t(1-t)} \sin\left(\frac{2\pi(1+\varepsilon)}{t+\varepsilon}\right), \quad \varepsilon = 0.05 \quad (3.14)$$

$$f(t) = \sum_{j=1}^{11} h_j K(t-t_j), \quad K(t) = \frac{1+\text{sgn}(t)}{2} \quad (3.15)$$

$$t_j = (0.1, 0.13, 0.15, 0.23, 0.25, 0.40, 0.44, 0.65, 0.76, 0.78, 0.81)$$

$$h_j = (4, -5, 3, -4, 5, -4.2, 2.1, 4.3, -3.1, 2.1, -4.2)$$

$$f(t) = 4 \sin(4\pi t) - \text{sgn}(t-0.3) - \text{sgn}(0.72-t) \quad (3.16)$$

$$f(t) = \sum_{j=1}^{11} h_j K\left(\frac{t-t_j}{\omega_j}\right), \quad K(t) = (1+|t|)^{-4} \quad (3.17)$$

$$t_j = t_{\text{Blocks}}$$

$$h_j = (4, 5, 3, 4, 5, 4.2, 2.1, 4.3, 3.1, 5.1, 4.2)$$

$$\omega_j = (0.005, 0.005, 0.006, 0.01, 0.01, 0.03, 0.01, 0.01, 0.005, 0.008, 0.005)$$

**Table 3.1** Denoising results of four special shape signals based on the AFD

Method	SNR of filtered result (dB)			
	Doppler	Blocks	Heavysine	Bumps
Wavelet transform	<b>12.98</b>	11.56	13.97	17.45
EMD	11.03	11.67	10.88	<b>18.35</b>
AFD	12.28	<b>15.72</b>	<b>19.57</b>	16.63

## CHAPTER IV DENOISING BASED ON THE AFD

### 4.1 TECHNIQUE OF THE DENOISING METHOD BASED ON THE AFD

Generally, a noisy ECG signal can be modeled as the summation of an ideal noiseless signal  $f(t)$  and separate independent noise  $n(t)$  [11]:

$$f_{noise}(t) = f(t) + n(t). \quad (4.1)$$

Although the noiseless signal is fixed from trial to trial, the noise term represents intrinsic variability, which may arise from a number of separate sources. In addition, Eq. (4.1) is very similar with Eq. (3.1). According to the characteristic of the AFD, decomposition components are distributed from high energy to low energy. Therefore, if the energy of the noise is smaller than the energy of the pure signal, there should be a such decomposition level  $N$  that the first  $N$  mono-components can be used to approximate the pure signal. The approximation of the original signal can be expressed by

$$s_r(t) = 2 \operatorname{Re} \{ \tilde{G} \} - \langle G_1, e_{\{a_1\}} \rangle \quad (4.2)$$

where

$$\tilde{G}(t) = \sum_{n=1}^N \langle G_n, e_{\{a_n\}} \rangle B_n(e^{jt}). \quad (4.3)$$

The technique of the denoising process based on the AFD is similar with the wavelet transform and the EMD. First, the AFD decompose signals to mono-components. Then some mono-components that contains original pure signals' components are filtered out to reconstruct the pure signals. The only difference is that the AFD has a very rigorous mathematical foundation. It decomposes signals based on their energy distribution. Therefore, mono-components are obtained from high energy to low energy one by one. Thus, the judgment of which mono-components should be selected to reconstruct pure signals can be the decomposition level  $N$ . If the threshold decomposition level is denoted as  $\varepsilon$ , the process is shown in Fig. 4.1.

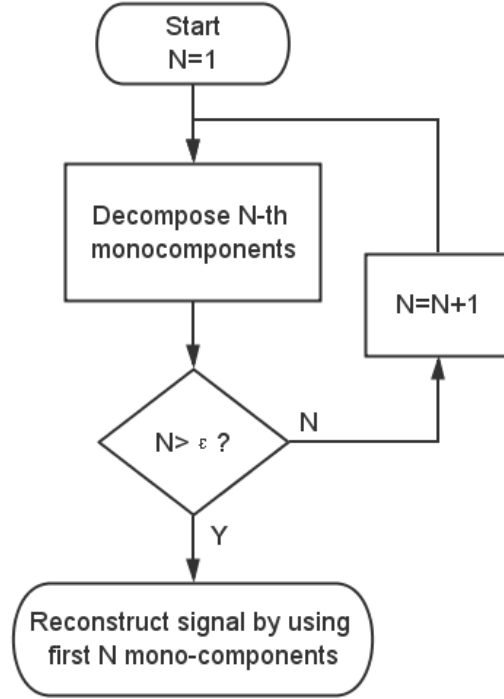


**Fig. 4.1** Denoising process based on the AFD with the threshold decomposition level  $\varepsilon$ .

However, most of the time, the threshold of the decomposition level  $N$  is still difficult to be determined. Therefore, I propose the AFD-based denoising method based on a judgment based on the estimated signal-to-noise ratio (SNR). It is able to stop the recursive AFD process automatically to get the denoising result and the suitable decomposition level. This judgment is defined by SNR in decibel. The definition of the SNR is shown in Eq. (4.4). If  $\text{SNR}_e$  denotes the estimated SNR of the noisy signal  $s(t)$ , Eq. (4.5) can be used to show the energy relationship between the noisy signal  $w(t)$  and the pure signal  $s_p(t)$ . For the ideal situation that all noise is in the remainder, the reconstructed signal  $s_r(t)$  will only contain the original signal. In other words, the energy of  $s_r(t)$  will be equal to the energy of the original signal  $s_p(t)$  in the ideal case. According to Eq. (3.2) and Eq. (3.8), we can use Eq. (4.6) to express the energy of the reconstructed signal. Combining Eq. (4.5) and Eq. (4.6), in the ideal case, the energy relationship between the noisy signal and the reconstructed signal can be expressed in Eq. (4.7) which can be used to be the judgment.

$$\text{SNR} = 10 \log_{10} \frac{\|s_p(t)\|^2}{\|w(t)\|^2} \quad (4.4)$$

$$\frac{\|s(t)\|^2}{\|s_p(t)\|^2} = 1 + \frac{1}{10^{\text{SNR}_e/10}} \quad (4.5)$$

$$\|s_r(t)\|^2 = 2 \sum_{n=1}^N |\langle G_n, e_{\{a_n\}} \rangle|^2 - |\langle G_1, e_{\{a_1\}} \rangle|^2 \quad (4.6)$$

$$\frac{\|s(t)\|^2}{2 \sum_{n=1}^N |\langle G_n, e_{\{a_n\}} \rangle|^2 - |\langle G_1, e_{\{a_1\}} \rangle|^2} = 1 + \frac{1}{10^{\text{SNR}_e/10}} \quad (4.7)$$

#### 4.2 IMPLEMENTATION OF THE DENOISING METHOD BASED ON THE AFD

In practice, Eq. (4.7) is difficult to be achieved. To make this judgment practical, it is necessary to find the relationship between decomposition level  $N$  and the energy of the reconstructed signal. The standard remainder  $R_N(t)$  in Eq. (3.1) has a characteristic [28]:

$$\|R_N\| \leq \frac{M}{\sqrt{N}} \quad (4.8)$$

where  $M$  is defined by  $\sum_{k=1}^{\infty} |c_k| \leq M$ . As the decomposition level  $N$  increases, the energy of the standard remainder  $R_N(t)$  decreases. Combining Eq. (3.8) and Eq. (4.7), it can be seen that the energy of the reconstructed signal  $s_r(t)$  increases as the decomposition level  $N$  increases. Therefore, before getting the threshold  $N$  that is able to make Eq. (4.7) successful, the ratio of the the noisy signal's energy  $\|s(t)\|^2$  to the reconstructed signal's energy  $2 \sum_{n=1}^N |\langle G_n, e_{\{a_n\}} \rangle|^2 - |\langle G_1, e_{\{a_1\}} \rangle|^2$  will be larger than the ideal energy ratio  $1 + \frac{1}{10^{\text{SNR}_e/10}}$ . Therefore, Eq. (4.9) can be used to determine if the denoising process can be finished in real situation. When the AFD is used to decompose a signal, all mono-components are found from  $n = 1$  to  $N$  one by one. Once Eq. (4.9) is reached, the decomposition process should be stopped. If the decomposition process is continued, more noise will be included into  $s_r(t)$ . If the decomposition process is stopped before Eq. (4.9) is reached, more energy of the original signal will be lost from  $s_r(t)$ .

$$\frac{\|s(t)\|^2}{2 \sum_{n=1}^N |\langle G_n, e_{\{a_n\}} \rangle|^2 - |\langle G_1, e_{\{a_1\}} \rangle|^2} \leq 1 + \frac{1}{10^{\text{SNR}_e/10}} \quad (4.9)$$

For the program of the denoising method, Two set of data should be inputted: the noisy signal data and its corresponding estimated SNR. Then according to this estimated SNR, the ideal energy ratio  $1 + \frac{1}{10^{\text{SNR}_e/10}}$  can be obtained. Then when the recursive AFD

process is running, the energy ratio  $\frac{\|s(t)\|^2}{2\sum_{n=1}^N |\langle G_n, e_{\{a_n\}} \rangle|^2 - |\langle G_1, e_{\{a_1\}} \rangle|^2}$  of every decomposition level should be checked. Whenever the energy ratio is larger than idea energy ratio, the AFD process will be stopped. The filtered results should be reconstructed by all obtained mono-components. This total process is shown in Fig. 4.2. The program flow chart is shown in Algorithm 1.

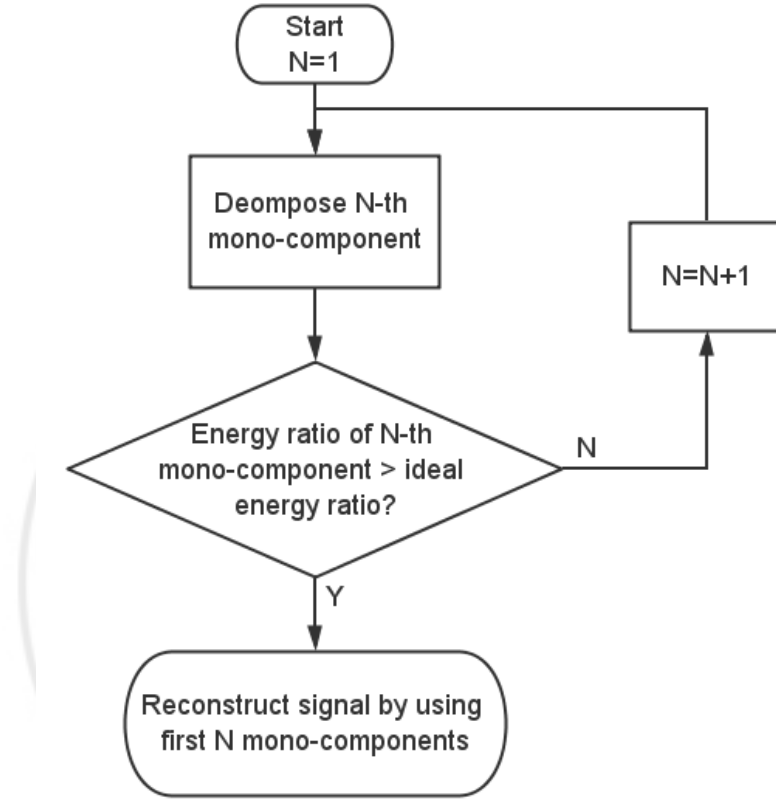


**Fig. 4.2** Flow chart of the denoising method based on the AFD.

---

**Algorithm 1** Denoising procedure based on the AFD

---

**Input:**  $s(t)$ : noisy ECG signal;  $\text{SNR}_e$ : estimated SNR of  $s(t)$

- 1: Initialize  $a_1 = 0$ ,  $N = 1$  and  $G(t) = G_1(t) = s(t)$ ;
- 2:  $e_{\{a_1\}}$  and  $B_1 \leftarrow \frac{\sqrt{1-|a_1|^2}}{1-\bar{a}_1 e^{jt}}$ ;
- 3:  $G_2 \leftarrow (G(t) - \langle G_1, e_{\{a_1\}} \rangle e_{\{a_1\}}) \frac{1-\bar{a}_1 e^{jt}}{e^{jt}-a_1}$ ;
- 4:  $a_2 \leftarrow \arg \max \left\{ \left| \left\langle G_2, \frac{\sqrt{1-|a_2|^2}}{1-\bar{a}_2 e^{jt}} \right\rangle \right|^2 : a_2 \in \mathbb{D} \right\}$ ;
- 5:  $e_{\{a_2\}} \leftarrow \frac{\sqrt{1-|a_2|^2}}{1-\bar{a}_2 e^{jt}}$ ;
- 6:  $B_2 \leftarrow \frac{\sqrt{1-|a_2|^2}}{1-\bar{a}_2 e^{jt}} \frac{e^{jt}-a_1}{\sqrt{1-|a_1|^2}} B_1$ ;
- 7: Let  $N = 2$ ;
- 8:  $ER \leftarrow \frac{\|s(t)\|^2}{2 \sum_{n=1}^2 |\langle G_n, e_{\{a_n\}} \rangle|^2 - |\langle G_1, e_{\{a_1\}} \rangle|^2}$ ;
- 9: **while**  $ER > 1 + \frac{1}{10^{\text{SNR}_e/10}}$  **do**
- 10:  $G_{N+1} \leftarrow (G_N(t) - \langle G_N, e_{\{a_N\}} \rangle e_{\{a_N\}}) \frac{1-\bar{a}_N e^{jt}}{e^{jt}-a_N}$ ;
- 11:  $a_{N+1} \leftarrow \arg \max \left\{ \left| \left\langle G_{N+1}, \frac{\sqrt{1-|a_{N+1}|^2}}{1-\bar{a}_{N+1} e^{jt}} \right\rangle \right|^2 : a_{N+1} \in \mathbb{D} \right\}$ ;
- 12:  $e_{\{a_{N+1}\}} \leftarrow \frac{\sqrt{1-|a_{N+1}|^2}}{1-\bar{a}_{N+1} e^{jt}}$ ;
- 13:  $B_{N+1} \leftarrow \frac{\sqrt{1-|a_{N+1}|^2}}{1-\bar{a}_{N+1} e^{jt}} \frac{e^{jt}-a_N}{\sqrt{1-|a_N|^2}} B_N$ ;
- 14: Let  $N = N + 1$ ;
- 15:  $ER \leftarrow \frac{\|s(t)\|^2}{2 \sum_{n=1}^N |\langle G_n, e_{\{a_n\}} \rangle|^2 - |\langle G_1, e_{\{a_1\}} \rangle|^2}$ ;
- 16: **end while**
- 17:  $s_r \leftarrow 2 \operatorname{Re} \left\{ \sum_{n=1}^N \langle G_n, e_{\{a_n\}} \rangle B_n \right\} - \langle G_1, e_{\{a_1\}} \rangle$ ;

**Output:**  $s_r$ : reconstructed filtered result;  $N$ : final decomposition level

---



## CHAPTER V SIMULATION RESULTS

This part is used to verify the Algorithm 1 and show the effect of the Algorithm 1 for the ECG denoising. Simulations are carried out in the MATLAB software. In these simulations, two types of ECG signals are used: a artificial ECG signals and real ECG signals. The artificial ECG signal generated by a ECG model [22] is used to verify the denoising principle shown in Chapter 4, while some real ECG signals from the MIT-BIH Arrhythmia Database [14, 23] are used to compare filtered results using the AFD with the ones using the Butterworth lowpass filter, the wavelet transform, the EMD and the ensemble empirical mode decomposition (EEMD). The main AFD program is provided by Qian, which can be found in [26]. For each type of signals, two types of noise is added. First type of noise is the additive Gaussian white noise which is a basic type of noise model. Second type of noise is a combination of two real noise records – the muscle artifact record and the electrode motion record from the MIT-BIH Noise Stress Test Database [14, 24].

### 5.1 ARTIFICIAL ECG SIGNAL

#### 5.1.1 ADDITIVE GAUSSIAN WHITE NOISE

A synthetic ECG generator is used to provide the artificial ECG signal. Details of this generator can be found in [22]. The sampling frequency is 256Hz. The heart rate is 60 beats per minutes. Three seconds data points of the generated ECG signal are used in this test. Additive Gaussian white noise is added to the signal resulting in a noisy signal with a 5.05dB SNR. The noisy signal is shown in Fig. 5.1. After using the proposed denoising method, the reconstructed filtered result can be obtained. Fig. 5.2 shows the reconstructed ECG signal with first 14 mono-components ( $N = 14$ ) against the original ECG signal. Comparing these two signals shown in Fig. 5.2, we can see the reconstructed signal almost reproduces the original ECG signal. In addition, the SNR of the reconstructed signal is increased to 9.61dB, which represents the improvement of 4.56dB to the noisy signal.

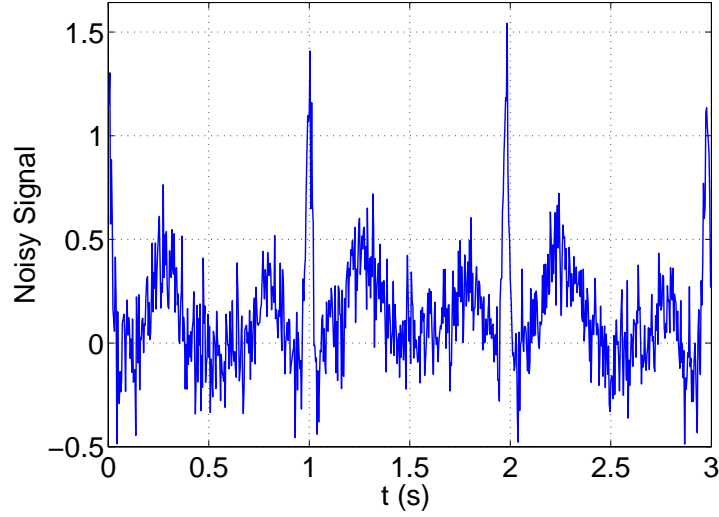


**Fig. 5.1** Noisy artificial ECG signal with additive Gaussian white noise that makes SNR 5.05dB.

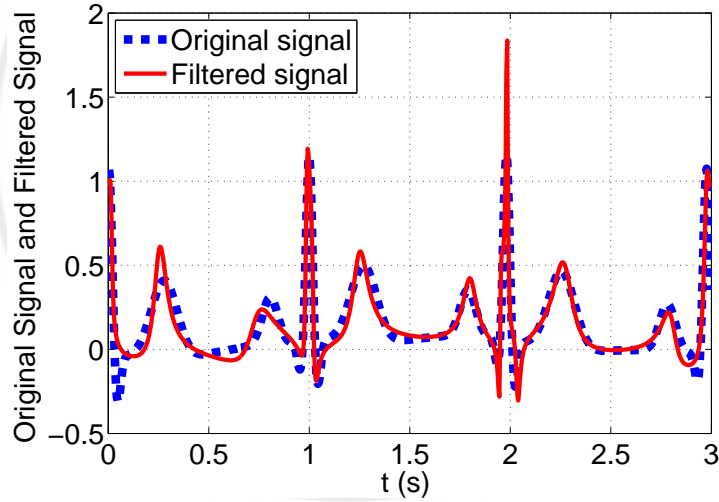


**Fig. 5.2** Original artificial ECG signal and filtered result for the additive Gaussian white noise simulation.

In Fig. 5.3, the cross symbols and circle symbols show the relationship between the ratio of the energy of the noisy signal  $\|s(t)\|^2$  to the energy of the reconstructed signal  $2\sum_{n=1}^N |\langle G_n, e_{\{a_n\}} \rangle|^2 - |\langle G_1, e_{\{a_1\}} \rangle|^2$  and the decomposition level  $N$  and the relationship between the SNR of the reconstructed result and the decomposition level  $N$ . The horizontal dashed line shows the ideal energy ratio  $1 + \frac{1}{10^{5.05/10}} = 1.313$ . The vertical dashed line shows the best decomposition level  $N = 14$  that is obtained by the decomposition process shown in Algorithm 1. According to Fig. 5.3, when the decomposition

level increases, the energy ratio will decrease. In addition, the absolute value of the slope of the energy ratio will also decrease. At  $N = 14$ , it is the first time that the energy ratio is smaller than the ideal value. At the same time, the SNR of the reconstructed ECG signal also gets its maximum point. These observations validate the proposed denoising principle of the AFD.

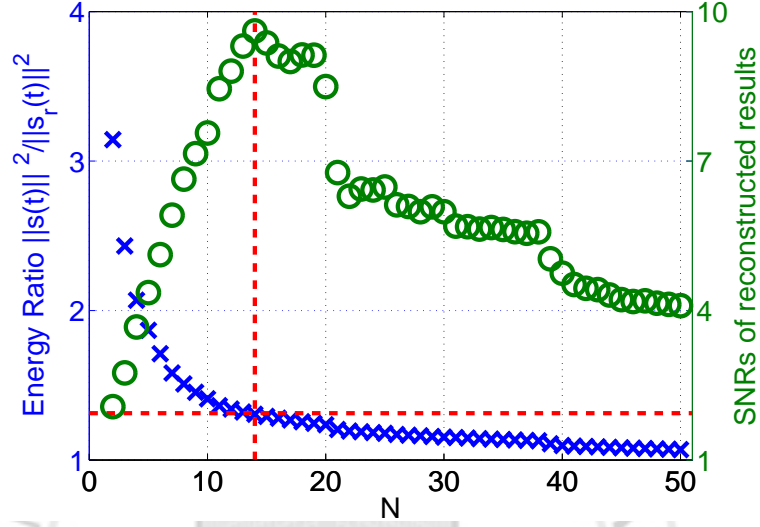


**Fig. 5.3** Energy ratio of the noisy signals to the reconstructed ECG signal and SNR of the reconstructed ECG signal for different  $N$  in the additive Gaussian white noise simulation.

### 5.1.2 COMBINATION REAL NOISE

The noise combination method is same as [3]. Two real noise records are taken from the MIT-BIH noise stress test database, the muscle artifact “ma” record and the electrode motion “em” record. The baseline wander (BW) in each record is eliminated by lowpass filtering. The total noise is

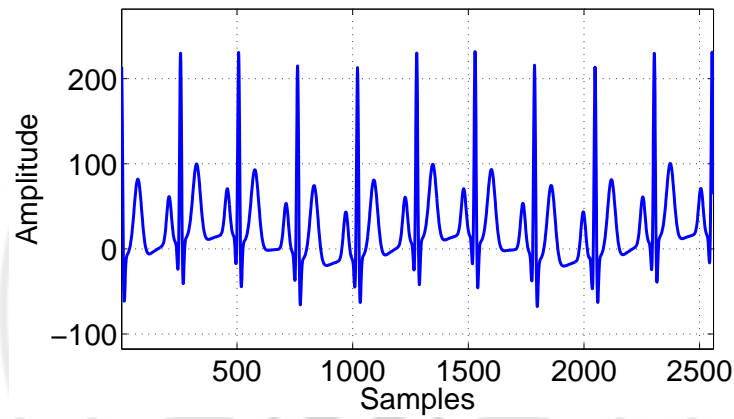
$$n(t) = k_1 n_{\text{ma}}(t) + k_2 n_{\text{em}}(t) \quad (5.1)$$

where  $n_{\text{ma}}(t)$  and  $n_{\text{em}}(t)$  are the “ma” and “em” BW free noise records, respectively [3]. Moreover,  $k_1$  and  $k_2$  are chosen to contribute with the same  $\text{SNR}_0$  [3]:

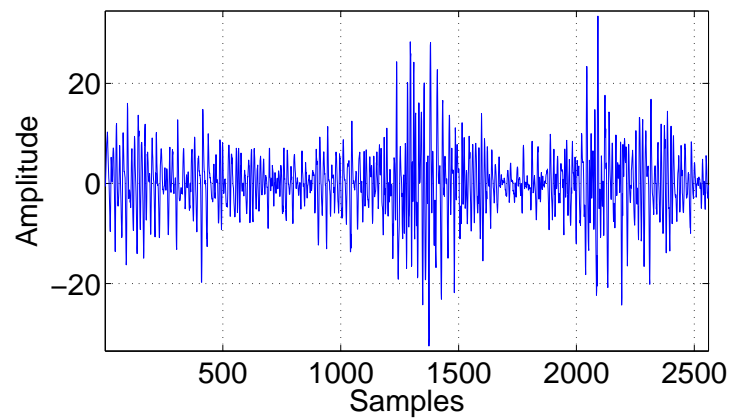
$$\text{SNR}_0 = \frac{\sum_{t=0}^{L-1} x^2(t)}{\sum_{t=0}^{L-1} [k_1 n_{\text{ma}}(t)]^2} = \frac{\sum_{t=0}^{L-1} x^2(t)}{\sum_{t=0}^{L-1} [k_2 n_{\text{em}}(t)]^2}. \quad (5.2)$$

Fig. 5.4 shows the set of signals involved in this simulation of the artificial ECG signal. In Fig. 5.4(a), The first 2560 samples the artificial ECG signal. The configuration

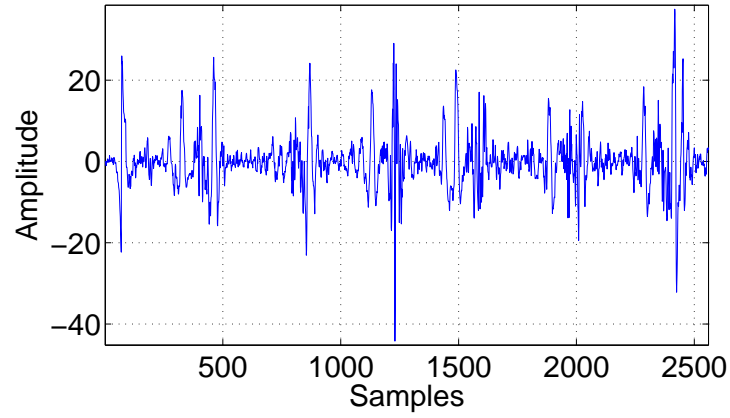
of this generator is the same as Section 5.1.1. The noisy signal is obtained by adding the noise in Fig. 5.4(d) attaining an SNR of 14.88dB. The noise signal is obtained as the summation of “ma” noise and “em” noise in Fig. 5.4(b) and Fig. 5.4(c), respectively, at an SNR of 18dB in both cases. The noisy signal is shown in Fig. 5.5. After the AFD-based denoising method, the reconstructed filtered result can be obtained. Fig. 5.6 shows the reconstructed ECG signal with first 65 mono-components ( $N = 65$ ) against the original clean ECG signal. Comparing these two signals shown in Fig. 5.6, it can be seen that the reconstructed signal almost reproduces the original ECG signal. In addition, the SNR of the reconstructed signal is increased to 17.54dB, which represents the improvement of 2.66dB to the noisy signal.



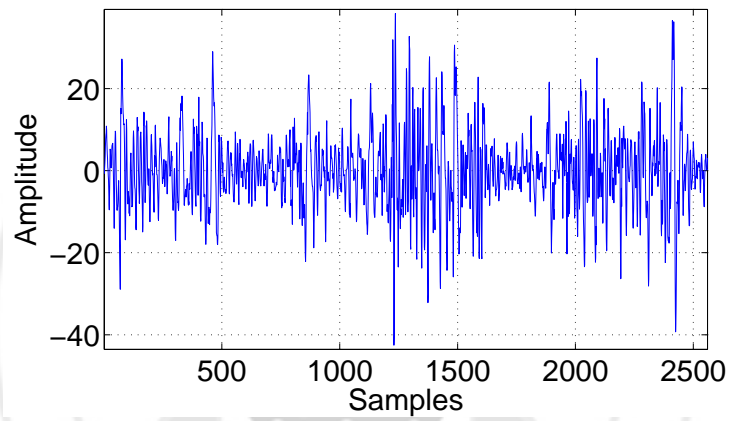
(a) Original artificial ECG signal.



(b) ‘ma’ noise at 18dB.



(c) 'em' noise at 18dB.



(d) Total noise at 14.88dB used to corrupt the original signal.

**Fig. 5.4** Set of signals for artificial ECG signal simulation of the combination real noise.

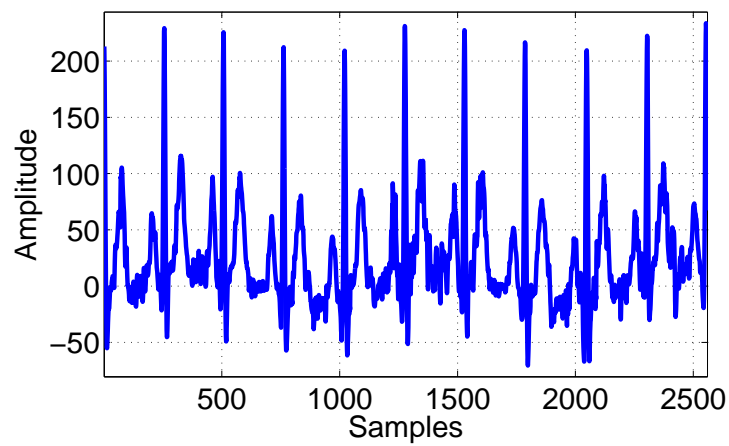


**Fig. 5.5** Noisy artificial ECG signal with the combination real noise that makes SNR 14.88dB.

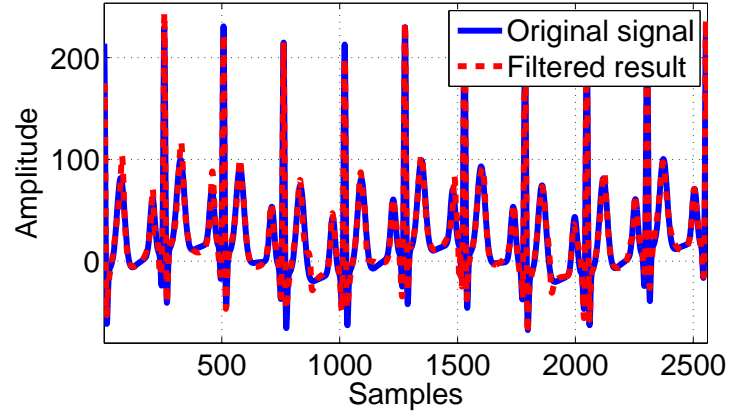


**Fig. 5.6** Original artificial ECG signal and filtered result for the combination real noise simulation.

In Fig. 5.7, the cross symbol and circle symbol show the energy ratios of the energy of the noisy signals to the energy of the reconstructed filtered results and SNRs of reconstructed filtered results for different decomposition level  $N$  respectively. The horizontal dashed line shows the ideal energy ratio  $1 + \frac{1}{10^{14.88/10}} = 1.03$ . The vertical dashed line shows the optimal decomposition level  $N = 65$  at which the SNR of the filtered result is maximum. According to Fig. 5.8, when the decomposition level increases, the energy ratio will decrease. In addition, the absolute value of the slope of the energy ratio will also decrease. At  $N = 65$ , it is the first time that the energy ratio is smaller than the ideal energy ratio. At the same time, the SNR of the filtered result also gets its maximum point. These observations validate the denoising principle of the AFD-based denoising method. Moreover, It shows that the AFD-based denoising method and the estimated-SNR-based judgment are able to be used to do real ECG noise reduction.

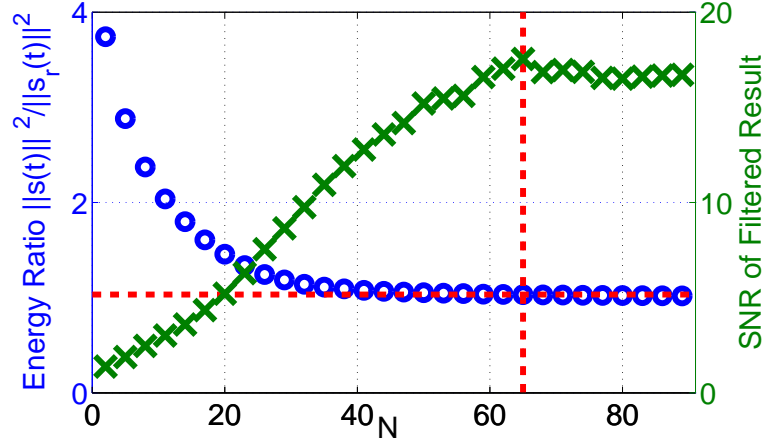


**Fig. 5.7** Energy ratio of the noisy signal to the reconstructed ECG signal and SNR of the reconstructed ECG signal for different  $N$  in the combination real noise simulation.

## 5.2 REAL ECG SIGNALS

### 5.2.1 ADDITIVE GAUSSIAN WHITE NOISE

To evaluate the proposed denoising method, four records from the MIT-BIH Arrhythmia Database, 100, 103, 105 and 119 are used. They were added Gaussian white noise, resulting in noisy signals with SNR ranging from 2dB to 15dB. For each SNR of the noisy signal, 50 independent runs are performed to get an average SNR of the reconstructed filtered signal. Results are shown in Fig. 5.8. We can see that the proposed denoising method is able to improve the SNR of the noisy ECG signal.

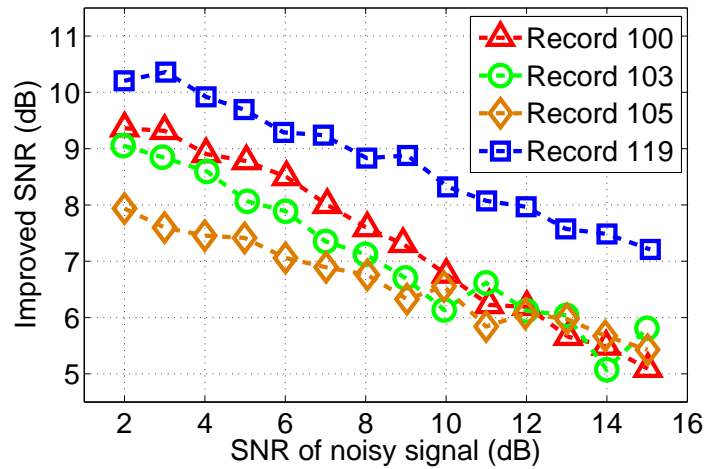


**Fig. 5.8** Improved SNRs of the filtered signals and corresponding SNRs of the noisy signals for four real signal records: 100, 103, 105 and 119 with additive Gaussian noise.

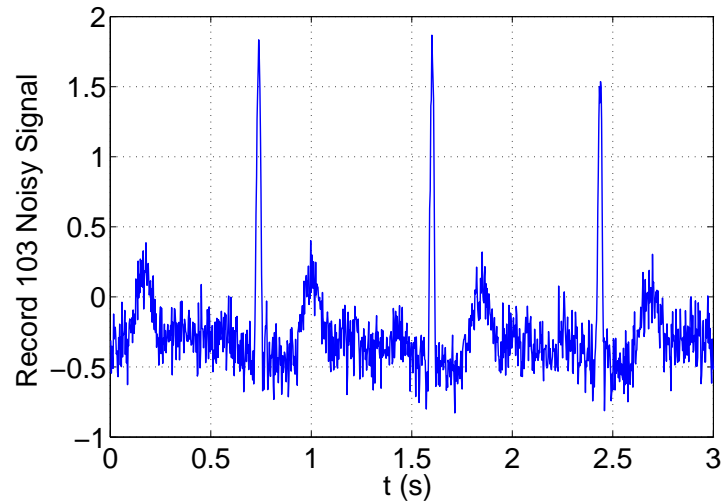


**Fig. 5.9** Record 103 signal with additive Gaussian white noise that makes the SNR 10dB.

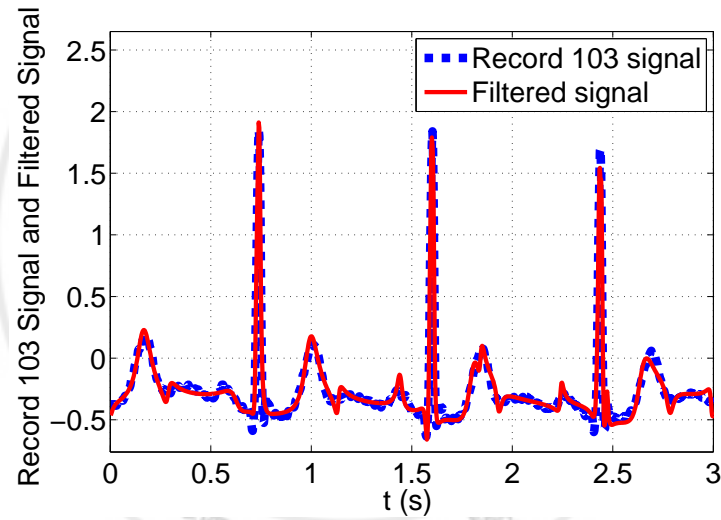


**Fig. 5.10** Original record 103 signal and reconstructed filtered result for the additive Gaussian white noise simulation.

We use three other denoising methods to compare with this proposed denoising method. Three methods are based on the wavelet transform, the EMD and the EEMD. First, the filtered results based on the wavelet transform from [12] are used to compare with the filtered results based on the AFD. In [12], the record 103 signal from the MIT-BIH Arrhythmia Database with additive Gaussian white noise is used. The same signal and the same type of noise were used in this test. Fig. 5.9 shows the noisy record 103 signal with additive Gaussian white noise that makes the SNR 10dB. After using the proposed denoising method, the filtered result can be obtained. Fig. 5.10 shows the



filtered result and the original record 103 signal. The filtered result almost reproduces the original ECG signal. The compared results are shown in Table 5.1. It can be found that the denoising method based on the AFD is able to provide best results for these four SNRs of noisy signals when compared with filtered results based on the wavelet transform.

**Table 5.1** Performance (SNR) comparison between filtered results based on the wavelet transform and the AFD for the additive Gaussian white noise simulation

SNR of the noisy signal (dB)	SNR of the filtered result (dB)		
	Wavelet transform with DB4	Wavelet transform with DB6	AFD
6.8	11.81	11.38	<b>13.35</b>
9.29	13.55	12.87	<b>14.36</b>
12.81	15.84	15.07	<b>17.81</b>
15.83	18.02	17.86	<b>18.36</b>

**Table 5.2** Performance (MSE) comparison between filtered results based on the EMD, the EEMD and the AFD for the additive Gaussian white noise simulation

Record No.	MSE of the filtered result		
	EMD	EEMD	AFD
101	126.9	97.4	<b>38.24</b>
102	83.3	60.0	<b>51.11</b>
103	189.4	147.0	<b>85.07</b>
104	151.6	109.5	<b>97.03</b>
105	180.6	128.1	<b>79.72</b>
106	245.6	192.5	<b>155.01</b>
107	771.7	<b>574.9</b>	702.14
108	103.2	76.9	<b>33.40</b>
109	237.2	179.7	<b>142.60</b>
201	67.1	38.6	<b>35.33</b>
202	131.3	76.3	<b>34.67</b>
203	279.7	<b>206.5</b>	623.88
205	72.5	55	<b>33.95</b>
207	129.7	99.9	<b>59.06</b>
208	361.2	<b>232.0</b>	262.60
209	140.3	103.3	<b>63.10</b>

Then filtered results of the method based on the EMD and the EEMD are used to compare with filtered results of the method based on the AFD. Filtered results of the method based on the EMD and the EEMD are from [8]. In [8], 16 records' signals from the MIT-BIH Arrhythmia Database with additive Gaussian white noise that makes SNR 10dB are used. We use same records' signals and add the same type of noise to do this simulation. Mean values of 50 runs' results are shown in Table 5.2. For these ECG signals, the method based on the AFD can provide best results most of the time when compared with filtered results based on the EMD and the EEMD.

### 5.2.2 COMBINATION REAL NOISE

To evaluate the performance of the proposed denoising method for real ECG noise, real ECG signals from the MIT-BIH Arrhythmia Database with the combination of real noise shown in Section 5.1.2 are used to do the simulations. Fig. 5.11 shows the noisy record 103 signal with the combination of real noise that makes SNR 14dB. After using the proposed AFD-based denoising method, the filtered result shown in Fig. 5.12 can be obtained. Comparing the original record 103 signal and the filtered result shown in Fig. 5.12, the filtered result almost reproduces the original ECG signal. The AFD-based denoising method is able to improve the SNR of the noisy ECG signal.

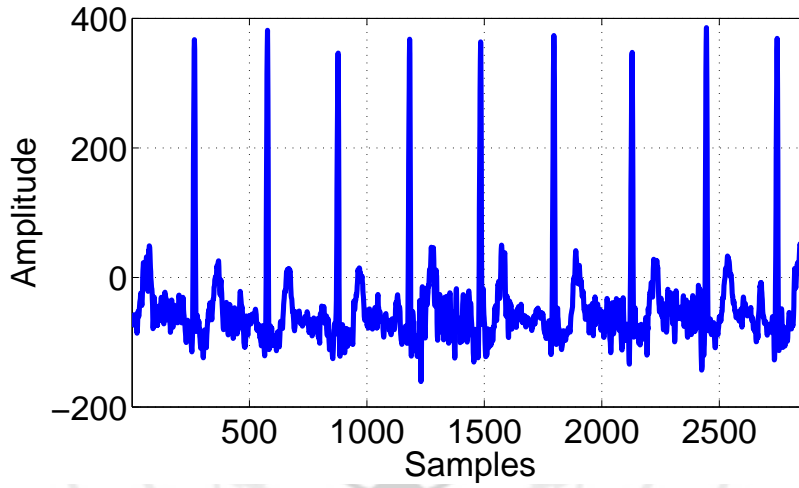


**Fig. 5.11** Record 103 signal with combination real noise that makes the SNR 14dB.

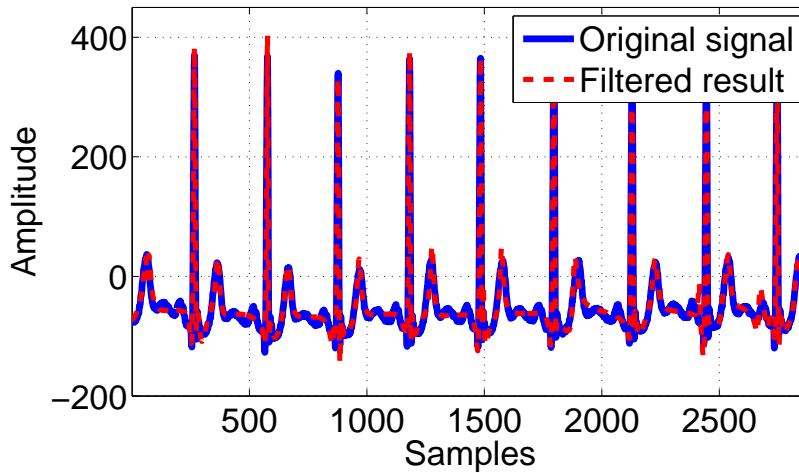


**Fig. 5.12** Original 103 signal and reconstructed filtered result for the combination real noise simulation.

To show the effectiveness of the AFD-based denoising method for real ECG noise reduction, three other denoising methods are used to compare with this AFD-based denoising method. These three methods are based on the Butterworth lowpass filter, the wavelet decomposition and the EMD. Their results are from [3]. In [3], 5 records' real ECG signals from the MIT-BIH Arrhythmia Database with the combination of real noise that makes SNR 6dB, 10dB and 14dB are used. We use the same records' signals and add the same type of noise to do this simulation. The comparing results are shown in Table 5.3 where  $SNR_{emd}$ ,  $SNR_{butt}$ ,  $SNR_{wt}$  and  $SNR_{AFD}$  denote the SNRs of the filtered results based on the EMD, the Butterworth lowpass filter, the wavelet transform and the AFD, respectively. It shows that the AFD-based denoising method almost performs better than the denoising method based on the EMD and the wavelet transform.

**Table 5.3** Performance (SNR) comparison between filtered results based on the EMD, the wavelet transform and the AFD for the combination real noise simulation

Record No.	SNR = 6dB				SNR = 10dB			
	$SNR_{emd}$	$SNR_{butt}$	$SNR_{wt}$	$SNR_{AFD}$	$SNR_{emd}$	$SNR_{butt}$	$SNR_{wt}$	$SNR_{AFD}$
100	<b>11.40</b>	5.22	6.14	9.55	<b>13.95</b>	7.33	10.15	13.44
103	9.85	3.58	6.15	<b>10.34</b>	12.90	4.92	10.16	<b>13.43</b>
105	9.62	5.53	6.14	<b>10.88</b>	11.94	7.89	10.14	<b>12.76</b>
119	<b>11.45</b>	6.48	6.14	10.81	14.71	9.63	10.14	<b>14.75</b>
213	<b>8.87</b>	4.45	6.13	7.96	11.89	10.14	10.13	<b>12.00</b>

Record No.	SNR = 14dB			
	$SNR_{emd}$	$SNR_{butt}$	$SNR_{wt}$	$SNR_{AFD}$
100	<b>16.75</b>	8.58	14.17	16.41
103	15.70	5.59	14.18	<b>16.37</b>
105	14.54	9.37	14.13	<b>16.28</b>
119	17.29	12.03	14.15	<b>17.81</b>
213	<b>14.74</b>	7.06	14.13	<b>14.74</b>

### 5.3 DISCUSSION

Normally, the proposed AFD-based denoising method shown in Algorithm 1 provides the optimal decomposition level  $N$ . In simulations of real ECG signals, some-

times, the optimal decomposition level  $N$  and provided  $N$  are not same. However, it is not a serious problem for ECG denoising. According to the relationship between the energy ratio and the decomposition level  $N$  shown in Fig. 5.3 and Fig. 5.7, if the optimal decomposition level  $N$  and the provided  $N$  are large enough, and their difference is not very large, the performances of filter results of these two cases should almost be same. For additive Gaussian white noise, Table 5.4 shows the differences between the optimal decomposition level  $N$  and the provided decomposition level  $N$  and the differences between performances under these two kinds of decomposition levels. For combination real noise, Table 5.5 where  $SNR_{se}$  is the provided decomposition levels of the Algorithm 1,  $SNR_{op}$  is the optimal decomposition level, and  $SNR_{diff}$  is the difference between  $SNR_{se}$  and  $SNR_{op}$  shows the differences between performances under these two kinds of decomposition levels. From these two tables, it is easily found that whether the the differences between the optimal decomposition level  $N$  and the provided decomposition level  $N$  or the differences between performances under these two kinds of decomposition levels are not very large.

**Table 5.4** Performance (MSE) under different decomposition level  $N$  for additive Gaussian white noise

<b>Record No.</b>	<b>Selected <math>N</math></b>	<b>MSE under selected <math>N</math></b>	<b>Optimal <math>N</math></b>	<b>MSE under optimal <math>N</math></b>
101	94	35.27	97	34.96
105	83	75.75	85	71.08
205	103	33.20	106	32.22
207	44	52.72	48	47.73

**Table 5.5** Performance (SNR) under different decomposition level  $N$  for the combination real noise

Record No.	SNR = 6dB			SNR = 10dB			SNR = 14dB		
	SNR <sub>se</sub>	SNR <sub>op</sub>	SNR <sub>diff</sub>	SNR <sub>se</sub>	SNR <sub>op</sub>	SNR <sub>diff</sub>	SNR <sub>se</sub>	SNR <sub>op</sub>	SNR <sub>diff</sub>
100	9.55	10.12	0.57	13.44	13.56	0.12	16.41	16.99	0.58
103	10.34	11.20	0.86	13.43	13.75	0.32	16.37	17.08	0.71
105	10.88	10.89	0.01	12.76	13.16	0.40	16.28	16.93	0.65
119	10.81	11.44	0.63	14.75	14.77	0.02	17.81	18.05	0.24
213	7.96	8.82	0.86	12.00	12.69	0.69	14.74	15.67	0.93

To obtain optimal results, sometimes we still need to adjust the decomposition level after the proposed denoising process. According to these simulations, two basic rules about how to adjust the threshold of the AFD can be found. According to [28], there is a relationship between the threshold  $N$  and stander remainder  $R_N$ :

$$\|R_N\| \leq \frac{M}{\sqrt{N}}. \quad (5.3)$$

As the threshold  $N$  increased, the stander remainder  $R_N$  will be decreased. And the decay rate is the negative root of the threshold  $N$ . When  $N$  is small,  $R_N$  will decreased very fast. From Eq. (3.1) and Eq. (3.6), the relationship between  $n$ -th mono-component and  $n$ -th stander remainder  $R_N$  can be found easily:

$$\|G_n(t)\|^2 = \|R_N\|^2 - \|R_{N+1}\|^2. \quad (5.4)$$

Combining Eq. (5.3) and Eq. (5.4), we can obtain

$$\|G_n(t)\|^2 \leq M^2 \left( \frac{1}{N} - \frac{1}{N+1} \right). \quad (5.5)$$

Since  $N$  only can be positive integer, the energy of  $n$ -th mono-component  $G_n(t)$  is decreased as the threshold number  $N$  increased. In other words, if first  $N$  mono-components are used to recovery the pure signal as shown in Eq. (4.2), this process is like a “high energy filter”. It will make sure that high energy components will be decomposed first from the noisy signal and added to the recovered signal. It implies two points: if we want to recover more energy, the threshold  $N$  needs to be increased; if the energy of noise is larger than that of the pure signal, it is difficult to recovery the pure signal from the noisy signal. From these two points, the first rule can be obtained:

*When the signal-to-noise ration (SNR) of the noisy signal is positive, for the noisy signal which has larger SNR, the larger threshold  $N$  is needed to filter most noise from the noisy signal.*

The second rule is related to global frequencies of mono-components. The AFD is a kind of adaptive decomposition method. It is able to show the time-frequency distribution of a signal. As Eq. (3.4) shows, for different time, mono-components may have different instantaneous frequencies. Therefore, it is difficult to determine the frequency relationship between two mono-components. However, it is easily shown that by writing  $B_n(e^{jt})$  as Eq. (3.4), there follows

$$\phi'_n(t) < \phi'_{n+1}(t), \quad t \in [0, 2\pi]. \quad (5.6)$$

According to this characteristic of  $B_n(e^{jt})$ , There still is a relationship related to the main frequency range between two mono-components: As the number  $n$  increased, the main frequency range of the mono-component  $s_n(t)$  will also increased. From this relationship, it can be found easily that the denoise process will look like a low pass filter if first  $N$  mono-components of the AFD are used to recovery the original pure signal. Then the second rule can be obtained:

*When the SNR of the noisy signal is positive, for the noisy signal which contains higher frequency components, the larger threshold  $N$  is needed to filter most noise from the noisy signal.*

Since single sinusoidal signals are easily used to show the frequency relationship, this type of signals is chosen to verify these two rules. The original signals  $f(t)$ 's are single sinusoidal signals which don't have phase difference and whose frequencies are from  $2Hz$  to  $20Hz$ . SNRs of noisy signals  $f_{noise}(t)$  are from  $-20dB$  to  $20dB$  after additive Gaussian white noise is added into the original signals  $f(t)$ 's. The AFD is used to decompose every noisy signal. For every decomposition level, the SNR of the reconstructed signal is calculated to find the optimal decomposition level. For every pair of  $f_{noise}(t)$  and  $f(t)$ , this kind of simulation will repeat 50 times to get the mean value of the these 50 optimal decomposition level  $N$ . The simulation result is shown in Fig. 5.13. From Fig. 5.13, the relationship between the optimal decomposition level  $N$ , the frequency of original signal and the SNR of the noisy signal is shown very clearly, which satisfy these two rules

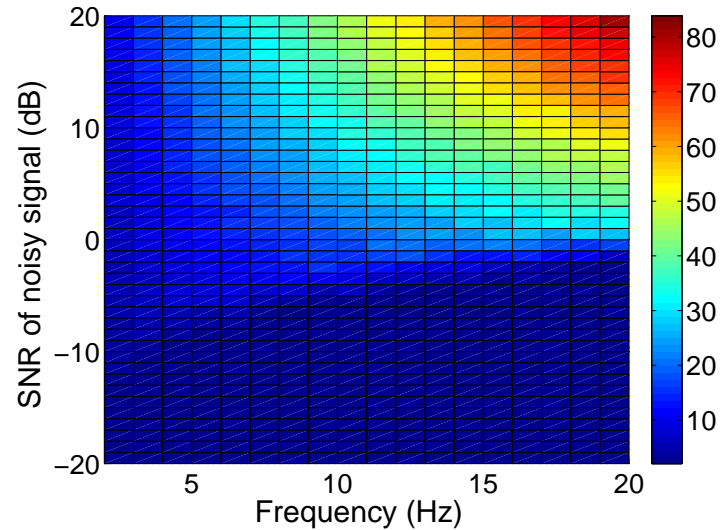


**Fig. 5.13** Optimal decomposition levels for different frequencies of original single sinusoidal signals and SNRs of noisy signals.

Although the AFD-based denoising method mostly can provide best filtered results in Table 5.2 and Table 5.3, sometimes, the filtered results of the EMD or the EEMD are better than the ones of the AFD. These special cases can be separated to two situations. For the first situation, the best filtered results are much better than the filtered result of the proposed method, i.e., the filtered results of the record 203 ECG signal shown in Table 5.2. The main reason that the filtered results of the proposed denoising method is not best in this situation is the limitation of the AFD for analyzing complex signals. Fig. 5.14 shows first ten seconds' record 203 ECG signal. It can be seen that this ECG signal contains too much small high frequency components. If this signal is considered as the original signal to let the AFD reconstruct it, the decomposition level needs to be more than 200, which cost large computation time and resources. In Table 5.2, to save simulation time, the maximum decomposition level is limited to 200. Although the final optimal filtered result of the proposed denoising method is better than the filter result based on the EEMD if the maximum decomposition level don't have any limitation, the performance of the proposed denoising method is still not good by considering the cost of the time and resources. This problem is mainly from the computation method and the program of the AFD. In the future, after optimizing the computation method and the program of the AFD, this problem may be able to be solved.



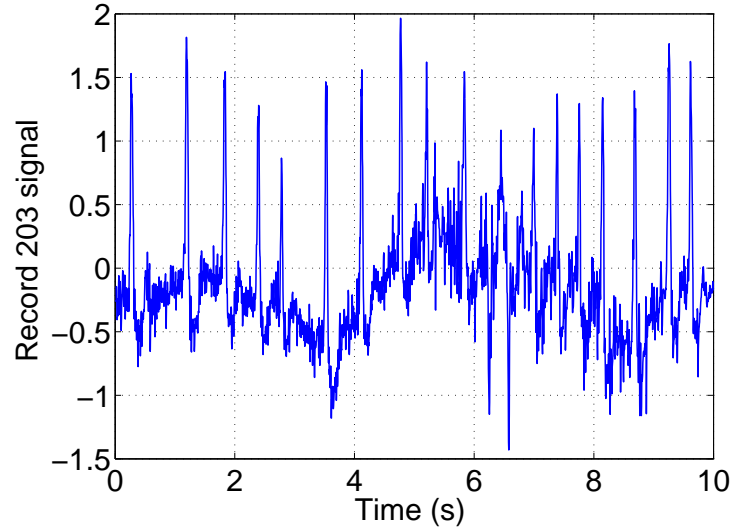


**Fig. 5.14** Record 203 ECG signal

For other special cases, they mainly belong to the second situation. the problem of this situation is mainly because the limitation of the denoising process. In this proposed denoising method, one estimated SNR is used to calculate the judgment. In other words, it assumes that the SNR is same in the whole data set. However, it is not true. the estimate SNR only shows an average value of the whole noisy signal. For ECG signals, most of the time, the actual SNRs of different parts are almost same as the average estimated SNR. Therefore, the proposed denoising method mostly perform better than other methods. However, sometimes, there are large differences between the actual SNRs and the estimated SNR. Then the performance of this AFD-based denoising method is reduced in this situation. For the EMD and the EEMD, they use windows to separate and protect different parts of ECG signals as shown in Section 2.3.3. Therefore, they don't have this problem. In the future, this protection window method may be also added into the AFD-based denoising method to solve this problem.

## CHAPTER VI CONCLUSION AND RECOMMENDATIONS FOR FUTURE RESEARCH

In this report, a denoising process based on the AFD for ECG signals is presented. The AFD mainly has two characteristics. First, it decomposes signals based on their energy distribution, which makes its convergence property good and make its decomposition components distribute from high energy to low energy. Second, its decomposition components are all mono-components whose phase derivatives are always positive. According to these characteristics, the AFD is suitable for the ECG signal denoising. To make this method practical in denoising process, a judgment is defined to determine if enough decomposition components have been obtained in the recursive AFD process to reconstruct filtered results. Based on this judgment, a AFD-based denoising method is proposed. To verify and demonstrate the effectiveness of this AFD-based denoising method, the artificial ECG signal and real ECG signals with additive Gaussian white noise, muscle artifact and electrode motion artifact are used to do simulations. From their simulation results, the proposed denoising method mostly can provide best performances when compared with denoising methods based on the butterworth lowpass filter, wavelet transform, the EMD and the EEMD, showing that the AFD is a promising tool for ECG signal denoising.

For the proposed denoising method based on the AFD, it is mainly related with the energy distribution of mono-components. In other words, there are still many characteristics of the AFD that have not been used. For the energy related characteristic, the AFD converges very fast. According to this property, the AFD may be able to be used to compress signals and images. Until now, the popular compressing technique is to use the Fourier transform, filter out high frequency components and keep Fourier series of low frequencies. This compressing method not only damage lots of original signals but also still need to store a large data of Fourier series. For the AFD, since it converges fast. Few components may be enough to present a very long signal or a very large image. Therefore, in the signal or imaging compressing area, the AFD may be also a promising tool. For another characteristic of the AFD, its mono-components only contain positive phase derivatives. This characteristics may be able to be used to

analysis the instantaneous frequency. The instantaneous frequency is very important for many fields. Getting a high resolution instantaneous frequency means that we can get accurate frequency information in a small time period. It will make the response time of many devices short and the running speed fast. For example, the main technique of the SSVEP control is the frequency analysis based on the Fourier transform. However, to get a accurate frequency information, the Fourier transform needs a very long data set. To catch this data set, the control process cost long time. Therefore, if the AFD can short the data collecting and analysis time, the SSVEP control will become fast. Even the instantaneous SSVEP control may also can be implemented. In summary, Many useful and powerful characteristics of the AFD have not been used. The AFD has a promising developing future.



## REFERENCES

- [1] Alfaouri, M. and Daqrouq, K., 2008. "ECG signal denoising by wavelet transform thresholding". American Journal of Applied Sciences, Vol. 5, No. 3, pp. 276-281.
- [2] Antoniou, A., 2006. Digital Signal Processing, 1st ed., McGraw-Hill, New York.
- [3] Blanco-Velasco, M., Weng, B. and Barner, K. E., 2008. "ECG signal denoising and baseline wander correction based on the empirical mode decomposition". Computers in Biology and Medicine, Vol. 38, No. 1, pp. 1-13.
- [4] Bouzid, A. and Ellouze, N., 2007. "Maximum error in discrete emd decomposition of periodic signals". Proceedings of the 15th IEEE International Conference on Digital Signal Processing (DSP), Cardiff, pp. 563-566.
- [5] Bronzino, J. D., 2000. The Biomedical Engineering Handbook, 2nd ed., CRC Press, Boca Raton.
- [6] Chacko, A. and Samit, A., 2012. "Denoising of ECG signals using empirical mode decomposition based technique". Proceedings of 2012 IEEE International Conference on Advances in Engineering, Science and Management (ICAESM), Tamil Nadu, pp. 6-9.
- [7] Chang, H. C., Lee, P. L., Yeh, C. L., Shyu, K. K. and Hsu, Y. Y., 2012. "Enhancing EEG signals of steady-state visual evoked potential using a noise-assisted multivariate empirical mode decomposition". Technical Report, the National Central University, Taiwan.
- [8] Chang, K. M. and Liu, S. H., 2011. "Gaussian noise filtering from ecg by wiener filter and ensemble empirical mode decomposition". Journal of Signal Processing Systems, Vol. 64, No. 2, pp. 249-264.
- [9] Deering, R. and Kaiser, J. F., 2005. "The use of a masking signal to improve empirical mode decomposition". Proceedings of the 2005 IEEE International Conference on Acoustics, Speech, and Signal Processing (ICASSP), Philadelphia, Vol. 4, pp. 485-488.

- [10] Donoho, D. L. and Johnstone, J. M., 1994. "Ideal spatial adaptation by wavelet shrinkage". Biometrika, Vol. 81, No. 3, pp.425–455.
- [11] Enderle, J. D. and Bronzino, J. D., 2012. Introduction to Biomedical Engineering. 3rd ed., Academic Press, Oxford.
- [12] Ercelebi, E., 2004. "Electrocardiogram signals denoising using lifting-based discrete wavelet transform". Computers in Biology and Medicine, Vol. 34, No. 6, pp. 479–493.
- [13] Graps, A., 1995. "An introduction to wavelets". Computational Science & Engineering, Vol. 2, No. 2, pp. 50–61.
- [14] Goldberger, A. L., Amaral, L. A. N., Glass, L., Hausdorff, J. M., Ivanov, P. C., Mark, R. G., Mietus, J. E., Moody, G. B., Peng, C. K. and Stanley, H. E., 2000. "PhysioBank, PhysioToolkit, and PhysioNet: components of a new research resource for complex physiologic signals". Circulation, Vol. 101, No. 23, pp. e215–e220.
- [15] Hahn, S. L., 1996. Hilbert Transforms in Signal Processing, Boston.
- [16] Huang, N. E., Shen, Z., Long, S. R., Wu, M. C., Shih, H. H., Zheng, Q., Yen, N. C., Tung, C. C. and Liu, H. H., 1998. "The empirical mode decomposition and the hilbert spectrum for nonlinear and non-stationary time series analysis". Proceedings of the Royal Society of London A: Mathematical, Physical and Engineering Sciences, Vol. 454, No. 1971, pp. 903–995.
- [17] Kabir, M. A. and Shahnaz, C., 2012. "Denoising of ECG signals based on noise reduction algorithms in EMD and wavelet domains". Biomedical Signal Processing and Control, Vol. 7, No. 5, pp. 481–489.
- [18] Karagiannis, A. and Constantinou, P., 2011. "Noise-assisted data processing with empirical mode decomposition in biomedical signals". IEEE Transactions on Information Technology in Biomedicine, Vol. 15, No. 1, pp. 11–18.
- [19] Lee, P. L., Chang, H. C., Hsieh, T. Y., Deng, H. T. and Sun, C. W., 2012. "A brain-wave-actuated small robot car using ensemble empirical mode decomposition-

- based approach”. IEEE Transactions on Systems, Man and Cybernetics–Part A: Systems and Humans, Vol. 42, No. 5, pp. 1053–1064.
- [20] Li, T., Li, Q., Zhu, S., and Ogihara, M., 2002. “A survey on wavelet applications in data mining”. ACM SIGKDD Explorations Newsletter, Vol. 4, No. 2, pp. 49–68.
- [21] Mandic, D. P., 2011: “Filter bank property of multivariate empirical mode decomposition”. IEEE Transactions on Signal Processing, Vol. 59, No. 5, pp. 2421–2426.
- [22] McSharry, P. E., Clifford, G. D., Tarassenko, L. and Smith, L. A., 2003. “A dynamical model for generating synthetic electrocardiogram signals”. IEEE Transactions on Biomedical Engineering, Vol. 50, No. 3, pp. 289–294.
- [23] Moody, G. B. and Mark, R. G., 2001. “The impact of the MIT-BIH Arrhythmia Database”. IEEE Engineering in Medicine and Biology Magazine, Vol. 20, No. 3, pp. 45–50.
- [24] Moody, G. B., Muldrow, W. and Mark, R. G., 1984. “A noise stress test for arrhythmia detectors”. Computers in Cardiology, Vol. 11, No. 3, pp. 381–384.
- [25] Oppenheim, A. V., Willsky, A. S. and Nawab, S. H., 1997. Signals and Systems, 2nd ed., Prentice-Hall Englewood Cliffs, NJ.
- [26] Qian, T. and Mai, W., 2012, “AFDs software”. Website, [http://www.fst.umac.mo/en/staff/documents/fsttq/afd\\_form/index.html](http://www.fst.umac.mo/en/staff/documents/fsttq/afd_form/index.html).
- [27] Qian, T. and Wang, Y. B., 2011. “Adaptive Fourier seriesa variation of greedy algorithm”. Advances in Computational Mathematics, Vol. 34, No. 3, pp. 279–293.
- [28] Qian, T. and Wang, Y., 2013. “Remarks on adaptive Fourier decomposition”. International Journal of Wavelets, Multiresolution and Information Processing, Vol. 11, No. 1, pp. 1–14.
- [29] Qian, T., Wang, Y. B. and Dang, P., 2009. “Adaptive decomposition into mono-components”. Advances in Adaptive Data Analysis, Vol. 1, No. 4, pp. 703–709.
- [30] Qian, T., Zhang, L. and Li, Z., 2011. “Algorithm of adaptive Fourier decomposition”. IEEE Transactions on Signal Processing, Vol. 59, No. 12, pp. 5899–5906.

- [31] Rangayyan, R. M., 2002. Biomedical Signal Analysis, IEEE press, New York.
- [32] Reddy, G. U., Muralidhar, M. and Varadarajan, S., 2009. "ECG de-noising using improved thresholding based on wavelet transforms". Internatinational Journal of Computer Science and Network Security, Vol. 9, No. 9, pp. 221–225.
- [33] Rilling, G., Flandrin, P. and Goncalves, P., 2003. "On empirical mode decomposition and its algorithms". IEEE-EURASIP Workshop on Nonlinear Signal and Image Processing NSIP, Vol. 3, pp. 8–11.
- [34] Rilling, G., 2007. "G. rilling's emd matlab program". Website, <http://perso.ens-lyon.fr/patrick.flandrin/emd.html>.
- [35] Sayadi, O. and Shamsollahi, M. B., 2005. "ECG denoising with adaptive bionic wavelet transform". Proceedings of the 27th Annual International Conference of the IEEE Engineering in Medicine and Biology Society (EMBC), Shanghai, pp. 6597–6600.
- [36] Sharpley, R. C. and Vatchev, V., 2006. "Analysis of the intrinsic mode functions". Constructive Approximation, Vol. 24, No. 1, pp. 17–47.
- [37] Schlurmann, T. 2001. "The empirical mode decomposition and the hilbert spectra to analyse embedded characteristic oscillations of extreme waves". Rogue Waves 2000, edition Infremer, ISBN: 2-84433-063-0, pp. 157–165.
- [38] Singh, O. and Sunkaria, R. K., 2013: "ECG signal denoising based on empirical mode decomposition and moving average filter". Proceedings of the 2013 IEEE International Conference on Signal Processing, Computing and Control (ISPCC), Solan, pp. 1–6.
- [39] Tikkanen, P., 1999. "Nonlinear wavelet and wavelet packet denoising of electrocardiogram signal". Biological Cybernetics, Vol. 80, No. 4, pp. 259–267.
- [40] Victor, 2012. "Introduction to the empirical mode decomposition method." Website, <http://www.mql5.com/en/articles/439>.
- [41] Weng, B., Blanco-Velasco, M. and Barner, K. E., 2006. "ECG denoising based on the empirical mode decomposition". Proceedings of the 28th Annual International

Conference of the IEEE Engineering in Medicine and Biology Society (EMBS),  
New York, pp. 1–4.

- [42] Wu, Z. H., 2010. “Wu’s emd matlab program”. Website, <https://code.google.com/p/matlab-analysis/source/browse/trunk/EEMD/emd.m?r=7>.
- [43] Wu, Z. H. and Huang, N. E., 2009. “Ensemble empirical mode decomposition: a noise-assisted data analysis method”. Advances in Adaptive Data Analysis, Vol. 1, No. 1, pp. 1–41.





## APPENDIX: RELATED PUBLICATIONS

- (1) Ze Wang, Chi Man Wong, Janir Nuno da Cruz, Feng Wan, Pui-In Mak, Peng Un Mak and Mang I Vai, “Adaptive Fourier decomposition approach for ECG denosing” submitted to Electronics Letters.
- (2) Ze Wang, Chi Man Wong, Janir Nuno da Cruz, Feng Wan, Pui-In Mak, Peng Un Mak and Mang I Vai, “Muscle and electrode motion artifacts reduction in ECG using adaptive Fourier decomposition” submitted to the 2014 IEEE International Conference on Systems, Man, and Cybernetics (SMC 2014).
- (3) Wei Chen, Ze Wang, Ka Fai Lao and Feng Wan, “Ocular artifact removal from EEG Using ANFIS” accepted by the 2014 IEEE International Conference on Fuzzy Systems (FUZZ-IEEE 2014)

